Progress in Neurobiology 264 (2026) 102943

Contents lists available at ScienceDirect

Progress in Neurobiology

journal homepage: www.elsevier.com/locate/pneurobio

Astrocytic α7 nicotinic acetylcholine receptors play an essential role in regulating glutamate dynamics and memory flexibility in the hippocampus

Maria Rosaria Tropea [a,b,1], Marcello Melone [c,d,1], Roberto Piacentini [e,f,1], Alessandro Di Spiezio [g], Manuela Tore [h], Roberta Carmela Trovato [a], Valeria Vacanti [a], Luca Bragina [c,d], Giulia Puliatti [e], Martina Albini [e], Beatrice Cannata [e,f], Sara Ben Abid [h], Nicole Tonesi [h], Angela Chiavegato [i], Micaela Zonta [g,j], Cristian Ripoli [e,f], Gabriele Losi [h,1], Claudio Grassi [e,f,1], Fiorenzo Conti [c,d,1,2], Daniela Puzzo [a,b,*,1]

[a] Dept. Biomedical and Biotechnological Sciences, University of Catania, Catania 95123, Italy
[b] Oasi Research Institute-IRCCS, Troina 94018, Italy
[c] Section of Neuroscience and Cell Biology, Dept. Experimental and Clinical Medicine, Università Politecnica delle Marche, Ancona 60020, Italy
[d] Center for Neurobiology of Aging, IRCCS INRCA, Ancona 60020, Italy
[e] Department of Neuroscience, Università Cattolica del Sacro Cuore, Rome 00168, Italy
[f] Fondazione Policlinico Universitario A. Gemelli, IRCCS, Rome 00168, Italy
[g] Neuroscience Institute, Section of Padova, National Research Council (CNR), Padova 41125, Italy
[h] Nanoscience Institute, CNR (CNR-NANO), Modena 41125, Italy
[i] Department Biomedical Science, University of Padova, Padova 35131, Italy
[j] Padua Neuroscience Center (PNC), University of Padova, Padova 35129, Italy

ARTICLE INFO

Keywords:
α7 nicotinic acetylcholine receptor
Hippocampus
Astrocyte
GLT-1
Glutamate dynamics
Synaptic plasticity
Memory flexibility

ABSTRACT

Astrocytes regulate hippocampal excitatory transmission by controlling glutamate dynamics, yet the contribution of cholinergic signaling to these processes remains poorly understood. Here, we investigated the role of astrocytic α7 nicotinic acetylcholine receptors (α7-nAChRs) in regulating glutamate homeostasis, synaptic plasticity, and memory flexibility in the hippocampus. Using ultrastructural analyses, functional imaging of glutamate, calcium, and sodium, electrophysiology, and behavioral approaches, we studied α7-nAChR knockout mice (α7KO) and an AAV-based mouse model enabling astrocyte-specific re-expression of α7-nAChRs (α7KI-astro). Electron microscopy revealed abundant α7nAChR expression in astrocytic processes at excitatory synapses in the hippocampal CA1 region. In α7KO mice, astrocytic calcium signaling and glutamate uptake were impaired. These alterations of glutamate dynamics were accompanied by reduced expression and altered localization of the glutamate transporter GLT-1, retraction of perisynaptic astrocytic processes, and deficits in synaptic fatigue, vesicle recycling, long-term depression, and memory flexibility. In α7KI-astro mice, calcium signaling, glutamate dynamics, synaptic plasticity, and memory flexibility were restored. Similarly, pharmacological enhancement of GLT-1 activity with ceftriaxone rescued both synaptic and behavioral deficits. Together, these findings identify astrocytic α7-nAChRs as critical regulators of glutamate homeostasis and hippocampal function, revealing a cholinergic mechanism through which astrocytes influence synaptic plasticity and cognitive flexibility.

1. Introduction

Alpha7-nicotinic acetylcholine receptors (α7-nAChRs) are homomeric ligand-gated ion channels whose activation typically results in the influx of Ca^{2+} ions that can contribute to membrane depolarization and modulate the release of several neurotransmitters, including glutamate. Among nicotinic receptor subtypes, α7-nAChRs are the most abundant in the adult mammalian brain and are highly expressed in the

* Corresponding author at: Dept. Biomedical and Biotechnological Sciences, University of Catania, Catania 95123, Italy.
E-mail addresses: danypuzzo@yahoo.it, daniela.puzzo@unict.it (D. Puzzo).
[1] Equal contribution
[2] Present address: European Brain Research Institute (EBRI) Rita Levi Montalcini Foundation, Viale Regina Elena 295, 00161 Rome, Italy

https://doi.org/10.1016/j.pneurobio.2026.102943
Received 14 January 2026; Received in revised form 24 June 2026; Accepted 20 July 2026
Available online 21 July 2026

hippocampus, where they contribute to learning and memory (Dani and Bertrand, 2007). Within hippocampal circuits, neuronal α7-nAChRs localize to both presynaptic and postsynaptic compartments (Fabian-Fine et al., 2001), where they facilitate glutamate release and modulate NMDA receptor activation, thereby influencing multiple forms of synaptic plasticity (Lin et al., 2010). Beyond neurons, α7-nAChRs are also expressed in astrocytes (Sharma and Vijayaraghavan, 2001; Shen and Yakel, 2012), where they participate in cholinergic modulation of neuron–glia communication (Pabst et al., 2016; Papouin et al., 2017) together with muscarinic AChRs (Chen et al., 2012; Takata et al., 2011). It is known that activation of astrocytic α7-nAChRs induces robust intracellular Ca^{2+} elevations and promotes the release of gliotransmitters, including glutamate and D-serine (Papouin et al., 2017; Pirttimaki et al., 2013; Sharma and Vijayaraghavan, 2001). However, the contribution of α7-nAChRs to astrocytic mechanisms that shape extracellular glutamate dynamics remains poorly understood.

Astrocytes regulate extracellular glutamate levels primarily through high-affinity Na^+-dependent transporters, of which GLT−1 (EAAT2) accounts for nearly 90% of total glutamate uptake in the forebrain (Takahashi et al., 2015). The efficiency of glutamate clearance depends not only on GLT−1 expression at the plasma membrane, but also on the fine architecture of perisynaptic astrocytic processes surrounding excitatory synapses (Lawal et al., 2022). Consequently, subtle alterations in GLT−1 localization or activity can markedly alter glutamate concentration in the synaptic cleft (Herde et al., 2020), affecting synaptic transmission, plasticity, and ultimately behavior. Moreover, because GLT−1 function is tightly coupled to Na^+ fluxes and astrocytic metabolic support, glutamate uptake is intrinsically linked to astrocytic excitability and ionic homeostasis (Danbolt, 2001).

Here, we aimed to define the physiological role of astrocytic α7-nAChRs in glutamate homeostasis at the hippocampus. To this end, we combined ultrastructural, imaging, electrophysiological, and behavioral analyses in α7 knockout (α7KO) mice and in a mouse model in which α7-nAChRs were selectively re-expressed in hippocampal astrocytes (α7KI-astro). We demonstrated that α7-nAChR dysfunction causes a spatial disorganization of GLT−1 and impairs glutamate uptake, leading to synaptic and behavioral deficits. These findings identify astrocytic α7-nAChRs as central modulators of glutamate dynamics linking cholinergic signaling to astrocyte-dependent control of hippocampal plasticity and memory flexibility.

2. Methods and materials

2.1. Animals and ethical approval

We used WT (C57BL/6 J; RRID:IMSR_JAX:000664) and α7KO mice (B6.129S7-Chrna7tm1Bay/J; RRID:IMSR_JAX:003232) purchased from The Jackson Laboratory. Colonies were established in the animal facilities at University of Catania, Università Cattolica del Sacro Cuore, University of Modena-Reggio Emilia and CNR Padova. Housing conditions were controlled maintaining stable hygrometric and thermic conditions (50%; 21°C ± 1°C) on 12 h light/dark cycle with ad libitum access to food and water. Mice were used at 3–6 months of age. Calcium and glutamate imaging, and behavioral studies were conducted on sex-balanced animals. For electrophysiological and electron microscopy experiments only male mice were used. All the experiments were performed according to the local Institutional Animal care and Use Committee (approval #119/2017-PR, #226/2021-PR, #944/2021-PR, #538/2023-PR) and the European Communities Council Directives (2010/63/EU). Experiments complied with the ARRIVE guidelines and were conducted to minimize animal suffering.

2.2. Molecular cloning and AAV vector production

Gibson Assembly Reaction (Gibson Cloning MasterMix, New England Biolabs, M5520A) was used to generate GFAP-CHRNA7-mRuby-WPRE-BGHpA flanked by AAV2 inverted terminal repeats (Supplementary Fig. 1**A**) as previously described (Ripoli et al., 2023). See Supplementary Material for details.

2.3. Generation and validation of α7KI-astro mouse model

We generated a mouse model selectively re-expressing α7-nAchRs in astrocytes, named α7KI-astro, through an AAV-based approach. At 12 weeks of age, mice received stereotaxic injections of the AAV vector into the dorsal hippocampus, specifically targeting the CA1, CA2, and CA3 regions.

Viral transduction specificity was assessed by immunofluorescence analyses using astrocytic (GFAP), neuronal (NeuN), and neural progenitor (Nestin) markers. Consistent with previous validation of this GFAP-driven construct (Puliatti et al., 2026), mRuby2 expression was restricted to astrocytes. No detectable viral transduction was observed in NeuN-positive neurons or Nestin-positive progenitor cells, and viral expression remained confined to the injected CA1–CA3 regions without detectable spread to the dentate gyrus. Detailed procedures are reported in the Supplementary Material and Supplementary Fig. 1.

2.4. Pre-embedding electron microscopy

Animals were deeply anesthetized and perfused with saline and a fixative mixture. Brains were removed, post-fixed, and cut in 50 μm serial parasagittal sections. For α7-nAChRs studies, rabbit antibodies raised against synthetic peptide within human CHRNA7 aa 450 to C-terminus conjugated to keyhole limpet haemocyanin were used, validated by employing control studies with α-BGT detection (Fig. 1 and Supplementary Table 1). For GLT−1 studies, rabbit antibodies raised against aa 559–573 of GLT−1a [GLT−1] rat C-terminus (Rothstein et al., 1994), validated in GLT−1 knock-out mice, were used (Omrani et al., 2009). Sections were incubated in a solution containing secondary biotinylated secondary antibodies, followed by avidin-biotin peroxidase complex and 3,3'diaminobenzidine tetrahydrochloride. They were post-fixed, dehydrated, embedded, and cut in ultrathin sections (~60 nm) that were examined by electron microscopy as described (Melone et al., 2019).

Data were collected, selected and captured to identify subcellular compartments and the distribution of α7-nAChRs, α-BGT, and GLT−1 at asymmetric synapses according to established criteria (DeFelipe et al., 1999; Melone et al., 2019; Peters et al., 1991). Distances between GLT−1 positive astrocytic processes and synaptic elements were measured using ImageJ. Distances < 300 nm were classified as perisynaptic and > 300 nm as extrasynaptic, as defined in previous studies (Parker et al., 2021). See Supplementary Material for a detailed description.

2.5. Primary cultures of murine hippocampal astrocytes

Primary cultures of hippocampal astrocytes were obtained from E18 WT and α7KO mice following procedure previously described (Li Puma et al., 2022). Briefly, after enzymatic and mechanical tissue dissociation, cells were suspended in a medium consisting of MEM with 3.7 g/L $NaHCO_3$ and 1.0 g/L D-glucose (DMEM), 10% FBS and 1% PSN, and cultured for 8–10 days. Astrocytes were plated at density of 10^5 cells on poly-L-lysine-coated 20-mm coverslips for Ca^{2+} and Na^+-imaging experiments.

2.6. High performance liquid chromatography (HPLC) measurements

HPLC measurements for extracellular glutamate determination was performed as previously described (Amorini et al., 2017; Piacentini et al., 2017). See Supplementary Material for a detailed description.

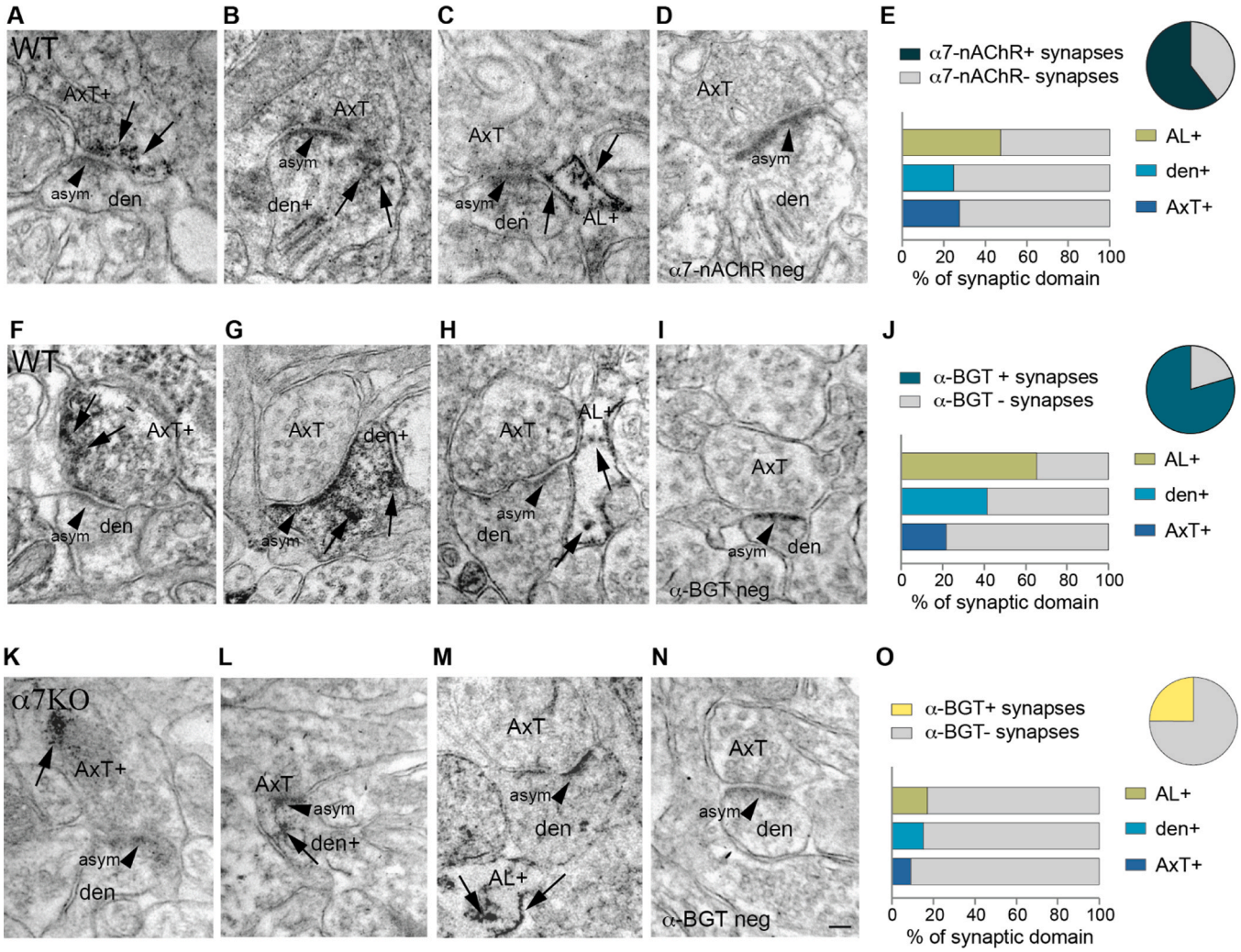

Fig. 1. α7-nAChRs ultrastructural distribution in CA1 area at excitatory synapses of stratum radiatum. A-C, Ultrastructural visualization of α7-nAChRs at asymmetric (asym) synapses in pre-embedded material from WT mice. In α7-nAChRs positive (+) synapses, dark immunopositive products (arrows) localize at axon terminals (AxT; A) forming asymmetric synaptic contacts (asym, arrowhead), in postsynaptic distal dendrites or spines (den; B), and in astrocytic leaflets contacting neuronal synaptic domains (AL; C); D, Example of α7-nAChRs negative (neg) synapse. **E,** Estimation of α7-nAChRs positivity rate reveals that 60.38% of identifiable asymmetric synapses are α7-nAChRs+. Distribution of α7-nAChRs at AxT, den and AL (for quantitative analysis, numerical values and statistics refer to Supplementary Table 1**a**). **F-H**, α-BGT detection in AxT (F), den (G), and AL (H) confirms the ultrastructural distribution of α7-nAChRs among synaptic domains. **I,** Example of α-BGT neg synapse. **J**, α-BGT positivity rate corresponds to 79.53% of total asymmetric synapses visualized. Distribution of α-BGT binding sites at AxT, den and AL (Supplementary Table 1**b**). **K-M**, Ultrastructural detection of α-BGT in AxT (K), den (L), and AL (M) in α7KO is dramatically decreased compared to WT. **N**, Example of α-BGT negative synapse. **O**, α-BGT positivity rate of asymmetric synapses is 24.91% (which corresponds to ~70% reduction compared to WT). Distribution of α-BGT binding sites at AxT, den and AL (Supplementary Table 1**b**). Scale bar: 100 nm.

2.7. Confocal Ca^{2+} and Na^{+} imaging

Primary cultures of astrocytes were loaded with either the Ca^{2+} and Na^{+} sensitive fluorescent dyes Fluo−4-AM or CoroNa™ Green-AM, respectively, in Tyrode's solution.

Intracellular Ca^{2+} transients were elicited by ATP stimulation. Images were acquired for 1 min around the stimulation period and continuously for 10 min, starting 5 min after stimulation. For each cell, the amplitude of all transients was measured and averaged. Frequency was calculated as the number of transients per 10 min, averaged across all cells. Similarly, Na^{+} transients were elicited by exposing CoroNa Green–loaded cells to L-glutamic acid.

The amplitude of Ca^{2+}/Na^{+} signals was estimated for each cell as follows: $\Delta F/F = (Ft - F_{pre})/(F_{pre} - F_{bgnd})$. A confocal system Leica TCS-SP5 was used for acquisition. See Supplementary Material for a detailed description.

2.8. Two-photon microscopy

Anesthetized animals were injected into the dorsal hippocampus of each hemisphere with AAV solutions containing GCaMP6f and TdTomato or CHRNA7-mCherry for calcium imaging; iGluSnFR.A184S and ACSF or CHRNA7-mCherry for glutamate imaging. Coronal or sagittal hippocampal slices were cut (300–350 μm thick), transferred into a submersion recording chamber and perfused with oxygenated solution containing a modified ACSF without NaPyruvate and L-ascorbic acid at room temperature or 32°C, for Ca^{2+} or glutamate experiments, respectively. We used two 2-photon laser scanning microscopes equipped with pulsed lasers tuned at 920 nm. Images were acquired with a water-immersion lens in CA1 *stratum radiatum*. For Ca^{2+} imaging, we used a 120 × 120 μm field of view at 1.53 Hz frame rate. Individual slices were perfused with TTX (0.5 μM) for at least 10 min before recording. For glutamate imaging, we acquired 200 × 300 μm areas at 25 Hz frame rate. Square current pulses to obtain a submaximal response were

applied. Multiple pulses were delivered at 20 Hz after a stable single pulse response was observed.

GCaMP6f fluorescence dynamics were extracted with the ROI-based MATLAB script AstroResp for astrocytic somata (Lia et al., 2023) and with the event-based script AQuA for the territories (Wang et al., 2019). iGluSnFR fluorescence dynamics were measured with Fiji ImageJ and expressed as $\Delta F/F_0$, where F_0 is the basal fluorescence before stimulus. Decay time constant τ was calculated with OriginPro after fitting with single exponential decay function of the average response normalized to the peak. See Supplementary Material for a detailed description.

2.9. Post-embedding electron microscopy

Sections were processed for an osmium-free embedding method (Melone et al., 2019). Thin sections (60 nm) were cut and mounted on 300 mesh nickel grids, processed for immunogold labeling, and incubated in a solution containing anti-GLT−1 antibody (for single labelling studies) or a mixture of anti-GLT−1 and α7-nAChRs primary antibodies. Grids were subsequently incubated with secondary antibodies conjugated to 12 nm (for single labelling) and 12 and 18-nm gold particles (for double-labelling), and then stained with uranyl acetate and Sato's lead. Ultrathin sections were examined and fields that included at least one immunolabeled astrocytic leafleats astrocytic process associated with an asymmetric synapse were acquired. Asymmetric synapses were selected based on a clear AZ /PSD complex. For determining the relative density of GLT−1 in single labeled studies, and GLT−1/ α7-nAChRs in double-labeled experiments, gold particles within labeled structures were counted, and areas were calculated using ImageJ. Gold particles were considered associated with plasma membrane if they were within 20 nm of the extracellular side of the membrane and cytoplasmic if they were $>$ 25 nm from the extracellular side of the membrane (Melone et al., 2019). See Supplementary Material for a detailed description.

2.10. Confocal microscopy

Confocal microscopy for the immunodetection of α1AR shown in Supplementary Fig. 3**B**, and for GLT−1 and VGLUT1 (Bragina and Conti, 2018) shown in Supplementary Fig. 4 is described in detail in Supplementary Methods.

2.11. Drugs

Ceftriaxone was dissolved in ddH2O and diluted in saline solution (0.9% NaCl) to a dose of 200 mg/kg in a final volume of 200 µL for intraperitoneal (ip) administration. Mice were treated for 8 consecutive days before behavioral and electrophysiological experiments. The dose and treatment duration were chosen based on previous works (Smaga et al., 2020).

2.12. Electrophysiological field recordings

Extracellular field recordings were conducted on 400 µm transverse hippocampal slices as described previously (Gulisano et al., 2019). Field excitatory post-synaptic potentials (fEPSPs) were recorded in CA1 *stratum radiatum* in response to Schaffer collateral stimulation. We used a low-frequency stimulation (LFS) protocol to induce LTD consisting of 900 pulses repeated at 1 Hz (intensity one and half of that of test pulses) (Babiec et al., 2014). Long term potentiation (LTP) was induced by a theta-burst stimulation (TBS) protocol consisting of three trains delivered at 15-s intervals as previously described (Tropea et al., 2021). For the study of synaptic fatigue, we exploited two stimulation protocols at 10 and 100 Hz. Recovery after depletion of the vesicle pool was elicited at the end of the 100 Hz stimulation by providing 7 additional pulses at an interval of 125 msec (Zhang et al., 2005). All synaptic fatigue protocols were performed in the presence of in 50 µM D-APV to avoid NMDA interference. See Supplementary Methods for a detailed description.

2.13. Behavioral studies

The Morris Water Maze was conducted as previously described (Tropea et al., 2024). Following the initial spatial learning phase, a reversal learning protocol was implemented (Kim et al., 1011). The hidden platform was relocated to the opposite quadrant and reversal learning took place over two additional days. 24 h after the final reversal learning trial, the probe test was repeated using the same quadrant division. To evaluate visual, motor, and motivational abilities, the time required to reach a visible platform was measured. Additional behavioral control experiments were performed to assess exploratory behavior in a novel environment, object exploration, and locomotor activity (Palmeri et al., 2016; Tropea et al., 2022). See Supplementary Material for a detailed description of all behavioral procedures.

2.14. Statistical analyses

All experiments were performed in blind with respect to treatment or genotype. Data were expressed as mean ± standard error mean (SEM). The level of significance was set at $p < 0.05$. Statistical analysis was performed by Systat 9, GraphPad Prism Software v. 10.1.1, SigmaPlot v.14.0 and Origin Pro 2023.

Based on preliminary analyses of normal distribution by Shapiro–Wilk normality test, we performed: (i) ANOVA for repeated measures to analyze LTD, synaptic fatigue, and MWM latency in the hidden and visible platform test; (ii) one-way ANOVA with Bonferroni's post-hoc correction for residual potentiation, MWM probe test, analysis of specific points of curves; (iii) two-tailed *t*-test when comparing two samples. For data with non-normal distribution, as assessed by D'Agostino and Pearson normality test, we used nonparametric contingency analysis with Fisher's test, Mann-Whitney test, Kruskal-Wallis ANOVA, Wilcoxon signed-rank test as indicated in the text. Statistical differences were established with $p < 0.05$ (*), $p < 0.01$ (**), $p < 0.001$ (***) and $p < 0.0001$ (****).

3. Results

3.1. α7-nAChRs are widely expressed at excitatory synapses of hippocampal CA1 area and preferentially sublocalized at astrocytic leaflets

We first investigated the ultrastructural distribution of α7-nAChRs in excitatory synapses of the hippocampal CA1 region using pre-embedding electron microscopy. Quantitative analysis of *stratum radiatum* in WT mice showed that 60.38% of identifiable asymmetric synapses (presence of a presynaptic axon terminal [AxT], distal postsynaptic dendrite or spine [den], and astrocytic leaflets contacting neuronal synaptic elements [AL]) exhibited α7-nAChRs immunoreactivity (ir) (Fig. 1**A-E**; Supplementary Table 1**a**).

α7-nAChRs ir was detected pre- and postsynaptically (AxT and den) and in AL (Fig. 1**A-C**). The positivity rate of α7-nAChRs in excitatory synapses of WT showed comparable expression in AxT and den, but AL+ was higher (47.38%) compared to AxT and den (Fig. 1**E**; Supplementary Table 1**a**).

We then analyzed α7-nAChRs ir in α7KO mice, characterized by similar levels of nicotine-binding sites but a dramatic decrease of α-BGT binding sites (Orr-Urtreger et al., 1997). In sections from α7KO mice we found a ~25% reduction of α7-nAChRs positivity rate of excitatory synapses compared to WT. Consistently to WT, the positivity rate of AxT and den was comparable, whereas that of AL was higher compared to AxT and Den (Supplementary Fig. 2; Supplementary Table 1**a**).

Next, we employed α-BGT ultrastructural detection to verify the positivity rate of α7-nAChRs and the distribution of α7-nAChRs among synaptic elements. In WT, the 79.53% of excitatory synapses were positive for α-BGT (Fig. 1**F-J**; Supplementary Table 1**b**). The α-BGT

detection localized, similar to α7-nAChRs, at AxT and den, with higher levels in AL compared to AxT and den (Fig. 1**J**; Supplementary Table 1**b**). In α7KO, consistent with the decrease in α-BGT binding sites (Orr-Urtreger et al., 1997), α-BGT detection at synapses dramatically decreased by approximately 70% compared to WT, with a general reduction across all synaptic domains (Fig. 1**K-O**; Supplementary Table 1**b**). Overall, these data demonstrate that α7-nAChRs are highly distributed in the hippocampus, especially in AL and confirmed the reduction of functional α7-nAChRs in α7KO mice.

3.2. Spontaneous and evoked Ca^{2+} transients are reduced in astrocytes from α7KO mice

Considering the abundant presence of α7-nAChRs in astrocytes and their role in Ca^{2+} signaling (Dani and Bertrand, 2007) we investigated Ca^{2+} transients in astrocytes within the CA1 *stratum radiatum* using 2-photon laser-scanning microscopy (2PLSM) on *ex vivo* coronal brain slices from WT and α7KO mice.

We recorded spontaneous Ca^{2+} activity in the presence of tetrodotoxin (TTX, 0.5 μM) to block neuronal action potentials. In WT mice, 49% of astrocytes showed spontaneous Ca^{2+} activity at the somata during the 2 min basal recording, while only 16% of α7KO astrocytes exhibited spontaneous activity (Fisher's exact test $p < 0.0001$; Fig. 2**A-B**, Supplementary Fig. 3). The amplitude of Ca^{2+} events was reduced by 80% in α7KO (Kruskal-Wallis ANOVA $p < 0.01$). In the surrounding territories, although most astrocytes were active in both WT and α7KO mice, a drastic reduction by 87% in the number of events was observed in slices from α7KO mice (Kruskal-Wallis $p < 0.01$; Fig. 2**C**).

To confirm that these effects were specifically linked to astrocytic α7-nAChRs, we generated an AAV vector encoding the functional α7-nAChR gene (CHRNA7) under the GFAP promoter for targeted astrocytic re-expression in α7KO mice, generating the α7KI-astro model (see methods and Supplementary Fig. 1). In α7KI-astro slices, spontaneous Ca^{2+} activity was fully restored in terms of active cells, signal amplitude, and frequency (Fig. 2**A-C**).

Next, we assessed Ca^{2+} activity evoked by noradrenaline (NA), which mobilizes calcium from the ER via α1 adrenergic receptor activation, and found similar activation in both WT and α7KO astrocytes (Fig. 2**D-E**). Consistently, α1Rs were similarly expressed in astrocytes of both genotypes (Supplementary Fig. 3). However, the amplitude of NA-induced Ca^{2+} response at the soma was significantly lower (87%) in α7KO astrocytes (Fisher's exact test, $p < 0.001$; Fig. 2**E**).

In addition, NA stimulation increased the frequency of Ca^{2+} events in WT astrocyte territories, but not in α7KO ones (Wilcoxon signed-rank test, $p < 0.05$; Fig. 2 **F**). Re-expression of α7-nAChRs in α7KI-astro mice fully restored NA-evoked Ca^{2+} activity in somata (Fig. 2**D-F**). Direct comparison of event frequency at territories upon NA stimulation between WT, α7KO and α7KI-astro mice revealed a significant difference between the groups (Kruskal-Wallis test, $p < 0.0001$), with post hoc Dunn's Test indicating a significant difference between WT and α7KO ($p < 0.0001$) and between α7KO and α7KI ($p = 0.004$; Fig. 2**F**).

To assess whether the Ca^{2+} alterations observed in hippocampal slices were also present in a controlled environment, we measured Ca^{2+} transients in cultured hippocampal astrocyte from WT and α7KO mice. Following 10-sec ATP stimulation (100 μM), the maximum amplitude of intracellular Ca^{2+} transients was significantly reduced in Fluo−4-loaded α7KO astrocytes compared to WT (Student's t test $p < 0.0001$; Fig. 2**G-H**).

Spontaneous transients recorded over 10 min after ATP stimulation showed a lower mean amplitude in α7KO astrocytes (Student's t test $p = 0.049$), while the frequency remained unchanged (Student's t test $p = 0.36$; Fig. 2**I-L, I-M**).

Taken together, these results confirm the crucial role of α7-nAChRs in shaping astrocytic Ca^{2+} dynamics in hippocampus.

3.3. Astrocytic α7-nAChR impairment alters glutamate dynamics affecting GLT−1-mediated glutamate uptake

To investigate the impact of astrocytic dysfunction on glutamate dynamics, we used 2PLSM to monitor extracellular glutamate at CA3-CA1 synapses in hippocampal slices expressing the SF-iGluSnFR-A184S sensor (Marvin et al., 2018) (Fig. 3**A**). Extracellular stimulation of Schaffer collaterals with single pulses evoked similar glutamate fluorescence transients in terms of decay time ($\tau = 0.48 \pm 0.03$ s, $R^2 = 0,97$ in WT vs 0.50 ± 0.02 s, $R^2 = 0,99$ in α7KO) and peak (unpaired Student's t test for all voltages $p > 0.05$) in both WT and α7KO mice (Fig. 3**B-C**).

However, with two pulses, α7KO slices showed a significantly larger increase in the extracellular glutamate peak (paired Student's t test for glutamate peak after one vs. two pulses: WT $p = 0.0013$; α7KO $p < 0.0001$; Fig. 3**D**) and a higher double-to-single pulse ratio compared to WT ($p = 0.0004$; Fig. 3**E**). In α7KI-astro slices, both the peak ($p = 0.0006$) and ratio were restored (α7KI vs WT: $p = 0.408$; α7KI vs α7KO: $p = 0.009$), suggesting that astrocytic α7-nAChRs are needed for maintaining glutamate dynamics.

Since the primary mechanism for glutamate clearance from the extracellular space involves the astrocytic transporter GLT−1, we performed additional 2PLSM experiments to investigate whether the increased glutamate peak found in α7KO slices was related to alterations in GLT−1-mediated uptake. Treatment with the GLT−1 blocker TBOA (10 μM for 10–12 min) increased the decay time constant τ of glutamate fluorescence after a single pulse especially in slices from α7KO mice (α7KO: $\tau = 0.96 \pm 0.06$ s, $R^2 = 0.99$; WT: $\tau = 0.70 \pm 0.06$ s, $R^2 = 0.97$ s) (Fig. 3**F-G**). Furthermore, TBOA significantly raised the glutamate peak fluorescence induced by single pulses only in α7KO slices (paired Student's t test $p = 0.023$; Fig. 3**H**). Therefore, in presence of TBOA, the 2/1 ratios were similar in the two genotypes ($p = 0.825$; Fig. 3**I**).

Because the GLT−1 function depends on Na^+ influx (Rao et al., 2015), we measured intracellular Na^+ transients induced by 20-s extracellular application of 100 mM L-glutamic acid in WT and α7KO cultured hippocampal astrocytes, as an index of glutamate uptake. The amplitude of Na^+ transients was significantly lower in α7KO astrocytes, with a reduction of about 25% (unpaired Student's t test $p = 0.0027$; Fig. 3**J-K**). Additionally, we found more glutamate into the supernatant of α7KO astrocytes than WT ones under resting condition ($p = 0.013$; Fig. 3**L**), thus suggesting a less efficient GLT−1-mediated uptake of the neurotransmitter.

Given the strong functional convergence of α7-nAChRs-mediated astrocytic defects and GLT−1-mediated impairment, we conducted double immunogold post-embedding studies to verify whether α7-nAChRs (12 nm gold particles) and GLT−1 (18 nm gold particles) were co-expressed in AL of intact synapses (Fig. 3**M-O**; Supplementary Table 2).

In double-labeled AL, gold particles coding for both α7-nAChRs and GLT−1 were detectable in the cytoplasm as well as in the membranes of the AL. Notably, of all AL colocalizing α7-nAChRs and GLT−1, 66.7% co-expressed both proteins at their membranes. The membrane pool of both proteins was higher than the cytoplasmic pool, indicating their preferential localization in the membrane domain (GLT−1: 44.53/μm^2 vs. 14.64/μm^2; α7-nAChRs: 38.66 vs 16.66/μm^2; $p < 0.001$ for both; Fig. 3**P**; Supplementary Table 2).

Overall, these findings suggest that α7-nAChR dysfunction impairs glutamate uptake via GLT−1, which colocalizes with α7-nAChRs.

3.4. Spatial organization of GLT−1 is altered in α7KO mice

Prompted by our functional data, we studied the ultrastructural organization of GLT−1. Pre-embedding electron microscopy of immunoperoxidase-labelled GLT−1 in the *stratum radiatum* showed that both WT and α7KO mice exhibited GLT−1 ir in astrocytic processes and neuronal profiles, including axons and axon terminals (Chen et al., 2004;

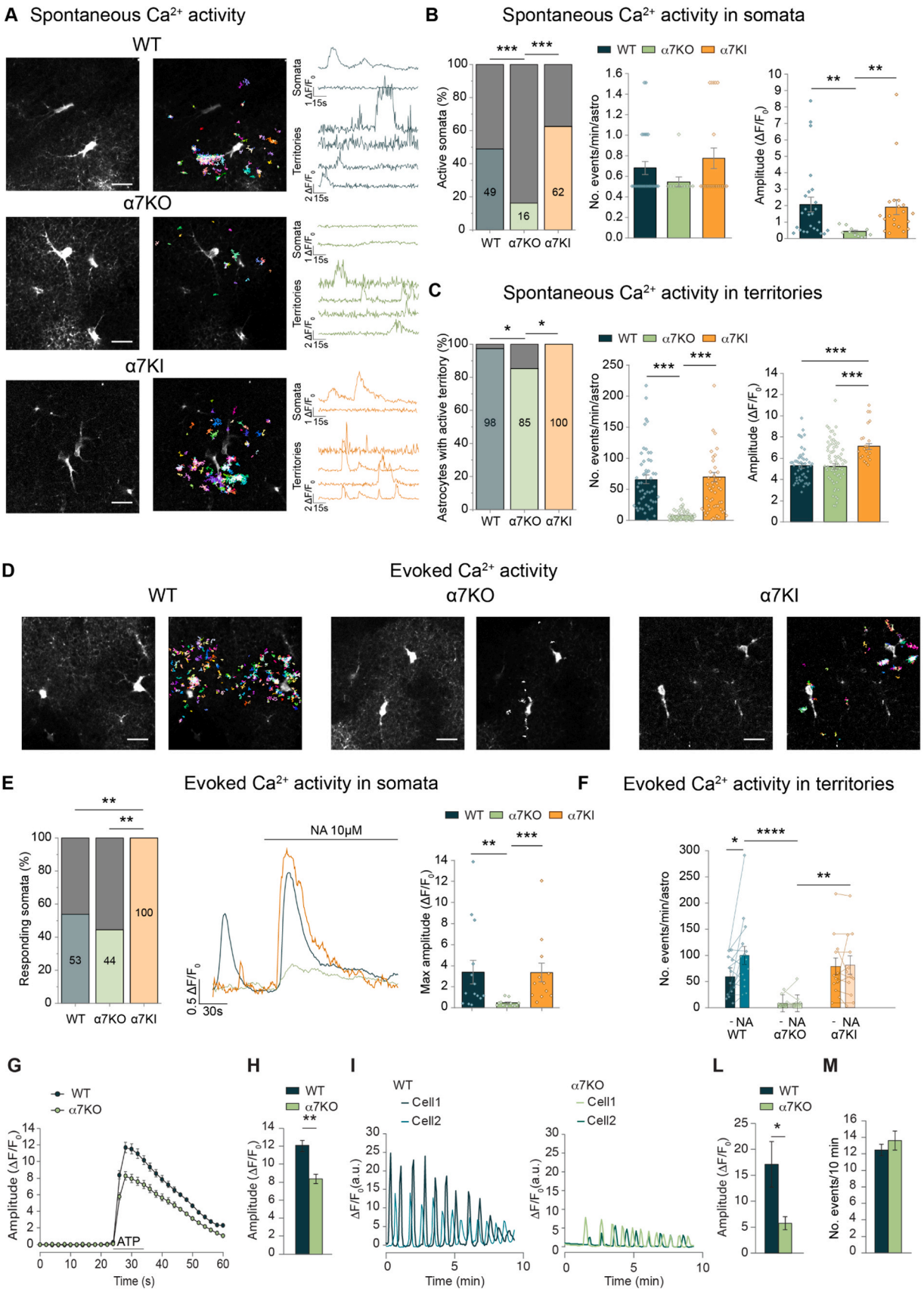

(caption on next page)

Fig. 2. α7KO hippocampal astrocytes display impaired Ca^{2+} activity. A, Representative Ca^{2+} imaging data. Left panels: maximum projection image of tdTomato fluorescence in hippocampal astrocytes. Right panels: merged image showing Ca^{2+} events in different colors on tdTomato reference image, and representative Ca^{2+} kinetics in astrocyte somata and territories. **B,** Left, astrocyte percentage exhibiting at least one spontaneous Ca^{2+} event. Middle, number of events. Right, amplitude of spontaneous Ca^{2+} events. n = 25 astrocytes from 12 slices from 7 WT mice, n = 11/10/5 α7KO, n = 20/5/3 α7KI. **C,** Same as in B but for territories. n = 51/12/7 WT, n = 58/10/5 α7KO, n = 32/5/3 α7KI. **D,** Same as A but for NA-evoked activity. **E,** Left, astrocyte percentage displaying NA-evoked Ca^{2+} activity. Middle, representative traces of Ca^{2+} responses upon NA perfusion. Left, max amplitude of somatic Ca^{2+} response. **F,** Number of Ca^{2+} events detected before (-) and after NA perfusion. n = 15/11/7 WT, n = 12/10/5 α7KO, n = 12/5/3 α7KI mice. Scale bar: 20 μm. **G,** Time course of intracellular Ca^{2+} transients elicited by ATP in WT and α7KO hippocampal astrocytes. **H,** Max amplitude of intracellular Ca^{2+} transients showed in (G) (n = 212 WT, 122 α7KO). **I,** Representative examples of spontaneous Ca^{2+} transients triggered in hippocampal WT and α7KO astrocytes 5 min after stimulation with ATP and recorded for 10 min (two cells for genotype). **L,** Mean amplitude of spontaneous Ca^{2+} transients in WT and α7KO astrocytes (n = 46 WT, 30 α7KO). **M,** Mean number of spontaneous Ca^{2+} transients observed in a time window of 10 min as in L. * $p < 0.05$; ** $p < 0.01$, *** $p < 0.001$, **** $p < 0.0001$.

Melone et al., 2009; Melone et al., 2019).

Quantitative analysis indicated that the density of GLT−1 + profiles was comparable in WT and α7KO mice (Mann Whitney test $p = 0.27$; Fig. 4**A-C**; Supplementary Fig. 4; Supplementary Table 3), and that GLT−1 ir at identifiable asymmetric synapses was reduced by 41% in α7KO mice (64.96% vs. 45.89%; $p < 0.0001$, Fisher's exact test; Fig. 4**D-G**; Supplementary Fig. 4; Supplementary Table 3). Further quantification of separate GLT−1 + AL and GLT−1 + AxT showed that the decrease in GLT−1 + synapses in α7KO mice correlated with a significant reduction in the proportion of GLT−1 + AL contacting asymmetric synapses (79.82% vs. 93.63% in WT) whereas that of GLT−1 + AxT was relatively increased ($p < 0.0001$ Fisher's exact test) (Fig. 4**H-K**; Supplementary Table 3).

Additionally, we measured the distance from the edges of the presynaptic active zone (AZ) and postsynaptic density (PSD) to the nearest astrocytic process at synapses with adjacent GLT−1 + AL (Parker et al., 2021). α7KO mice exhibited a lower proportion of perisynaptic astrocytic processes (distance <300 nm from the edge of the active zone/-postsynaptic density; 44.83% vs. 70.80% of WT) and a higher proportion of extrasynaptic processes (>300 nm) compared to WT mice (Fisher's exact test $p < 0.001$; Fig. 4**L-N**; Supplementary Table 3), suggesting that astrocytic processes are further away from the synaptic glutamate release sites in α7KO mice.

Next, the amount of GLT−1 at the membranes of GLT−1 + AL was evaluated through post-embedding analysis. The total density of GLT−1-coding particles in AL of α7KO mice was reduced by 27.6% (Mann-Whitney $p = 0.008$), with a decrease of 32.2% in the membrane pool of GLT−1 ($p < 0.001$; Fig. 4**O-Q**; Supplementary Table 4).

Taken together, these data demonstrate that α7-nAChR dysfunction leads to spatial alterations in GLT−1, with a displacement of astrocytic processes away from synaptic sites, which correlates with impaired glutamate uptake.

3.5. Dysfunction of GLT−1-mediated glutamate uptake impairs long-term depression and the vesicular recycling in α7KO mice

Having observed alterations in glutamate dynamics in young α7KO mice, we next explored whether the deletion of α7-nAChRs might affect long-term depression (LTD), a form of synaptic plasticity that reduces synaptic strength over time and is essential for neural circuit refinement. Electrophysiological field recordings at CA3-CA1 synapses showed a pronounced reduction in LTD in hippocampal slices from α7KO mice compared to age-matched WT controls ($F_{(1,11)} = 12.589$, $p = 0.005$), that was normalized in α7KI-astro mice ($F_{(1,12)} = 0.193$, $p = 0.668$ between WT and α7KI-astro; Fig. 5**A,C**).

In contrast, hippocampal long-term potentiation (LTP) was not altered in young α7KO mice, consistent with our previous observations that LTP deficits emerge only at later ages in this model (Tropea et al., 2021). These data are reported in Supplementary Figure 5.

Since the reduction of GLT−1 observed in α7KO synapses may contribute to the alterations in LTD, we investigated whether treatment with ceftriaxone, an antibiotic that has been shown to increase the expression of GLT−1 (Rothstein et al., 2005), could rescue this early synaptic dysfunction in α7KO mice. We found that sub-chronic administration of ceftriaxone (200 mg/kg for 8 days via i.p.) successfully restored LTD in hippocampal slices from α7KO mice ($F_{(1, 10)} = 24.366$, $p = 0.001$ between α7KO and α7KO treated with ceftriaxone) without affecting LTD in slices from WT mice (Fig. 5**B,C**).

We then studied possible alterations in presynaptic vesicular dynamics that may contribute to the disruption of LTD by impairing glutamate release. To this end, we evaluated vesicle recycling in CA3-CA1 synapses by employing two different protocols of synaptic fatigue (see methods for details). Post-synaptic responses were reduced during the 10 Hz synaptic fatigue, suggesting a faster depletion of readily available neurotransmitter vesicles at the presynaptic terminal in α7KO mice ($F_{(1,16)} = 10.04$, $p = 0.006$; Fig. 5**D**).

Next, we performed experiments of synaptic fatigue with a 100 Hz stimulation protocol to completely deplete synapses of the readily releasable pool (RRP) of glutamate vesicles. A significant difference was revealed between fatigue curves of WT and α7KO mice ($F_{(1,16)} = 13.037$, $p = 0.022$; Fig. 5**E**), suggesting a more rapid depletion of vesicle content in α7KO mice. Moreover, analysis of the recovery phase after the 100 Hz stimulation revealed a marked reduction in the refill rate in slices from α7KO mice compared to WT ($F_{(1,16)} = 6.458$, $p = 0.022$; Fig. 5**F**).

Alterations of synaptic fatigue tested both with the 10 Hz and 100 Hz protocols were restored in slices from α7KI-astro mice (10 Hz: $F_{(1,17)} = 0.001$, $p = 0.974$; $F_{(1,14)} = 1.529$, $p = 0.237$ between WT and α7KI-astro; Fig. 5**D-F**). Treatment with ceftriaxone was able to reestablish post-synaptic responses during 10 Hz ($F_{(1,16)} = 0.178$, $p = 0.678$; Fig. 5**G**) and 100 Hz synaptic fatigue ($F_{(1,15)} = 0.172$, $p = 0.685$; Fig. 5**H**), but it restored the refill rate only during the later phase of recovery (recovery at 875 ms: $F_{(3,30)} = 5.4$, $p = 0.004$; Bonferroni's post-hoc α7KO vs. α7KO treated with ceftriaxone: $p = 0.017$; α7KO treated with ceftriaxone vs. WT: $p = 1$; Fig. 5**I**).

These results indicate that deletion of α7-nAChR is associated with presynaptic changes that make the synapse less capable of responding to intense and repetitive stimulation, suggesting that vesicles deplete faster and need more time to be replenished.

3.6. α7KO mice display an impairment of spatial memory flexibility

Our previous studies have shown that young α7KO mice presented no memory alterations, while memory loss started at 12 months, along with deficits in LTP (Tropea et al., 2021). However, in the early stages, there may be alterations in memory flexibility associated with LTD changes. To evaluate this possibility, we used a revised version of the Morris Water Maze (MWM) test (Kim et al., 2011) illustrated in Fig. 6**A**. Consistent with our previous findings, both WT and α7KO mice performed similarly during the training sessions (Hidden 1–8) (Fig. 6**B**) and the probe trial on day 5 (Fig. 6**C**, left).

However, when the hidden platform was relocated to the opposite quadrant of the pool as part of a reversal learning protocol, α7KO mice showed a significantly longer latency to reach the new platform compared to WT mice (REV Hidden 1–4; $F_{(1,18)} = 17.478$, $p = 0.001$; Fig. 6**B**, right). This was further confirmed during the second probe trial, where α7KO mice continued to spend time a similar amount of time in the previous target quadrant, i.e., the one used in the first version of the probe trial, compared to the new quadrant ($F_{(3,26)} = 1.32$, $p = 0.283$

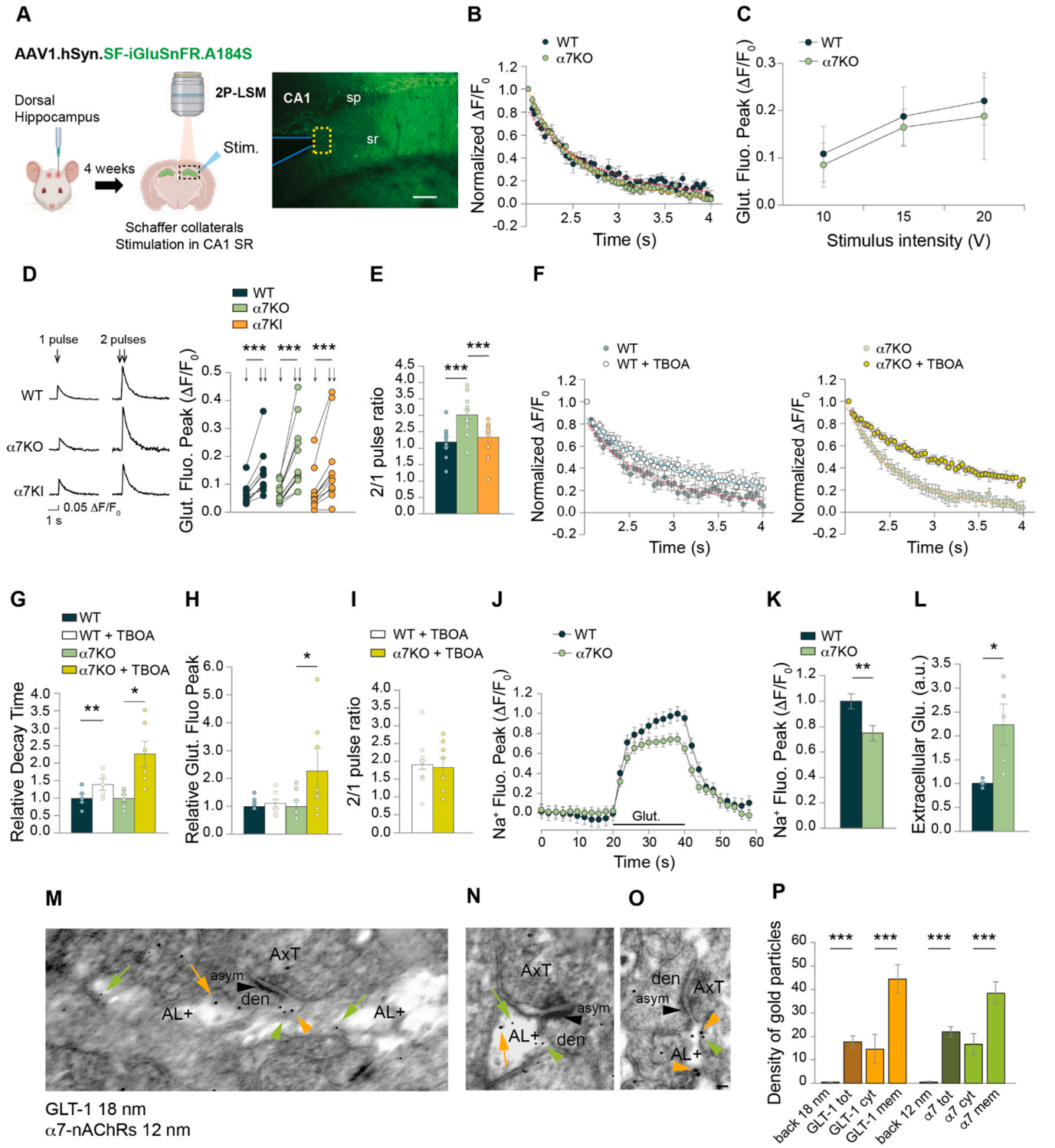

Fig. 3. Alterations of glutamate uptake in α7KO mice. A, AAV injection for the glutamate fluorescent sensor SF-iGluSnFR-A184S, Schaffer collaterals stimulation, and two-photon laser scanning microscopy (2PLSM). **B-C,** Decay time after a single pulse (n = 8 WT, 7 α7KO; dotted lines represent single exponential decay fitting) and (C) glutamate peak fluorescence (n = 6÷11/7÷8). **D,** Representative traces and graph of the glutamate peak after one and two pulses (n = 10/14/12). **E,** Ratio of the fluorescence peak of the second to the first pulse. **F,** Decay time in WT and α7KO mice treated with TBOA (n = 7/7; WT and α7KO curves as in B). **G-H,** Relative decay time constant (n = 5/6) and (H) peak (n = 7/8) of glutamate fluorescence in α7KO and WT with and without TBOA. **I,** Ratio between the second and first pulse after TBOA. **J,** Time course of intracellular Na^+ transients triggered by L-glutamic acid in cultured hippocampal astrocytes (n = 78/79). **K,** Mean maximum amplitude of intracellular Na^+ transients, as shown in J. **L,** Amount of extracellular glutamate in the culture medium of WT and α7KO hippocampal astrocytes. **M-O,** Representative examples of GLT−1/α7-nAChR colocalization in astrocytic leaflets of asymmetric synapses (AL+), where post-embedded GLT−1 and α7-nAChR are detectable in the cytoplasm (cyt; orange and green arrows point to GLT−1 and α7-nAChRs, respectively) and at the membranes (mem; orange and green arrowheads point to GLT−1 and α7-nAChRs, respectively). **P,** Total densities of GLT−1 and α7-nAChRs in AL and comparison of cyt and mem densities; see Supplementary Table 2). Scale bar: 50 nm. *p < 0.05; **p < 0.01; ***p < 0.001.

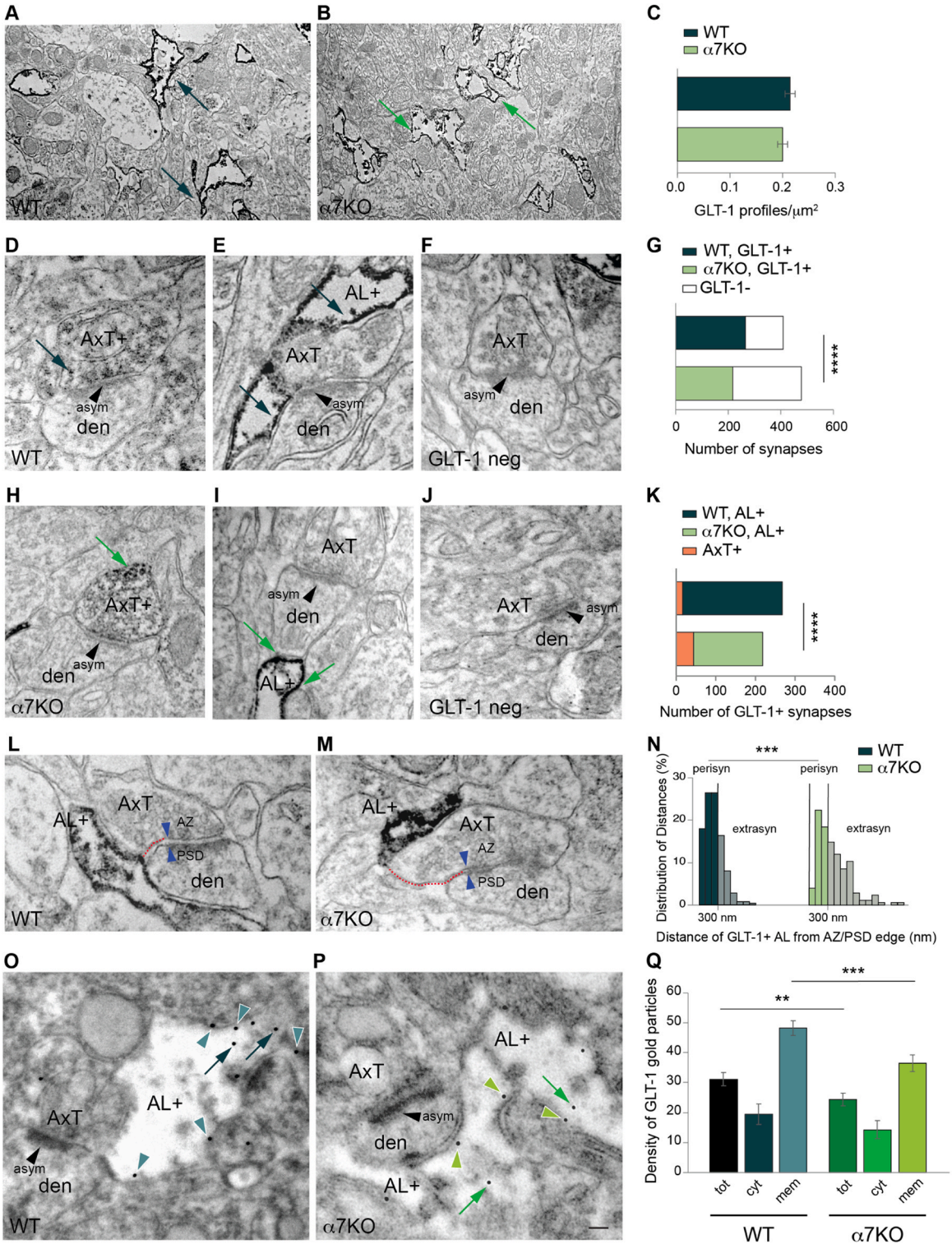

Fig. 4. Ultrastructural features of GLT−1 in *stratum radiatum* of WT and α7KO mice. A-C, Pre-embedded GLT−1 positive (+) profiles, characterized by dark electrodense immunopositive products (dark and light green arrows in A and B) in WT and α7KO mice. In C, graph showing the density of GLT−1 + in α7KO and WT. **D-G**, At GLT−1 + asymmetric (asym, arrowhead) synapses of both WT and α7KO, GLT−1 is detectable in axon terminals (AxT) making asymmetric synaptic contacts with the post-synaptic dendrites (den) and in astrocytic leaflets contacting neuronal synaptic domains (AL). In G, quantitative analysis of GLT−1 positivity rate of asymmetric synapses. **H-K**, Amount of GLT−1 + AL contacting asymmetric synapses and GLT−1 + AxT. **L-N**, For synapses containing adjacent GLT−1 + AL, proportion of perisynaptic (perisyn) AL (distance <300 nm from the edge of the active zone [AZ]/postsynaptic density [PSD]. Blue arrowheads indicate edges of the AZ/PSD to the nearest AL (see Supplementary Table 3). **O-Q**, Post-embedded GLT−1 in WT and α7KO is identifiable in the cytoplasm (arrows) and at the membranes of AL (arrowheads); in Q, graph the density of total (tot), membrane-associated (mem) and cytoplasmic (cyt) gold particles in AL of α7KO compared to WT (see Supplementary Table 4). Scale bar: 300 nm for A-B; 100 nm for D-F and H-J; 80 nm for L-M; 60 nm for O-P. $^{**}p < 0.01$; $^{***}p < 0.001$; $^{****}p < 0.0001$.

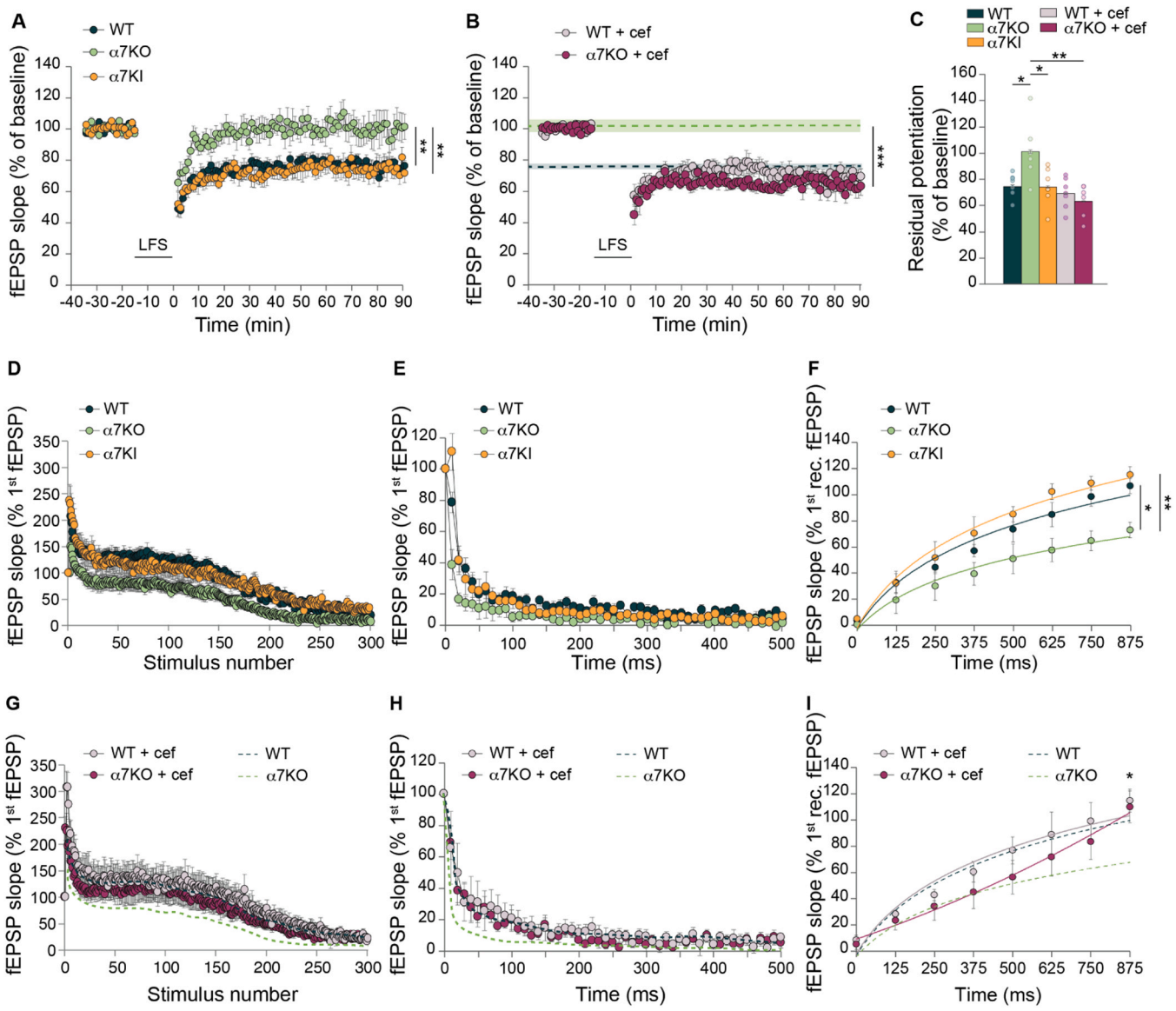

Fig. 5. Long-term depression and synaptic fatigue in α7KO mice. A, Long-term depression (LTD) recorded in hippocampal slices from WT, α7KO, and α7KO-astro mice (n = 7 slices from 7 WT mice; n = 6/5 α7KO; n = 7/5 α7KI-astro). **B,** Effects of a subchronic treatment with ceftriaxone (cef; 200 mg/kg i.p. for 8 days) in LTD (n = 6/6 WT + cef and 6/6 α7KO + cef). LFS = low-frequency stimulation (900 pulses 1 Hz). Dashed lines with shaded area represent the mean ± SEM of the last recorded point in slices from WT and α7KO mice shown in panel A. **C,** Analysis of residual potentiation (mean of the last 5 points of LTD recordings) in slices from WT, α7KO, α7KI-astro, α7KO treated with cef. **D,** Synaptic fatigue curves after 10 Hz stimulation in slices from WT (n = 9/5), α7KO (n = 9/6) and α7KI-astro mice (n = 10/6). **E,** Synaptic fatigue curves after 100 Hz stimulation in slices from WT (n = 9/5), α7KO (n = 9/5) and α7KI-astro mice (n = 7/5). **F,** Recovery phase after the 100 Hz fatigue protocol in slices from WT, α7KO and α7KI-astro mice. **G,** Effects of a treatment with ceftriaxone in 10 Hz synaptic fatigue in slices from WT (n = 8/4) and α7KO mice (n = 9/5). Dashed lines represent the trend of the curves for WT and α7KO shown in the respective panels. **H,** Effects of a treatment with ceftriaxone in 100 Hz synaptic fatigue in slices from WT (n = 7/4) and α7KO mice (n = 9/5). **I,** Recovery phase after the 100 Hz fatigue protocol in slices from WT and α7KO mice treated with cef. *p < 0.05; **p < 0.01.

comparing the time spent in quadrants; Bonferroni's p = 0.023 comparing the time spent in the new quadrant between WT and α7KO mice; Fig. 6**C**, right).

Re-expression of α7-nAChR in α7KI-astro mice prevented these early behavioral alterations in memory flexibility. Indeed, latency to reach the submerged platform was normalized ($F_{(1,18)}$= 3.648, p = 0.07 vs. WT) as well as the time spent in the new TQ (Bonferroni's p = 0.02 compared to α7KO and p = 1 compared to WT) (Fig. 6**B-C**). The rescue of memory flexibility was also obtained after treatment with ceftriaxone that normalized the performance of α7KO mice in reversal learning (REV Hidden 1–4; ($F_{(1,17)}$= 18.688, p < 0.0001, α7KO vs. α7KO treated with ceftriaxone; $F_{(1,17)}$= 0.465, p = 0.504, WT vs. α7KO treated with ceftriaxone; Fig. 6**D**) and second probe trial (Bonferroni's p = 0.188, WT vs. α7KO treated with ceftriaxone; Fig. 6**E**).

We also examined potential sex-dependent differences in behavioral performance by stratifying data according to sex. Although this analysis was limited by the relatively small number of animals, no significant sex-dependent effects were detected in the behavioral phenotype observed in WT, α7KO and α7KO-astro mice (Supplementary Fig. 6**A-B**) or in animals treated with ceftriaxone (Supplementary Fig. 6**C-D**).

A visible platform trial did not reveal any significant difference in the time to reach the platform between different genotypes or treatments (Supplementary Fig. 7 **A**). Additional behavioral control experiments revealed no differences between WT and α7KO mice in exploratory behavior of a novel environment, as assessed by a 5-min open field test, including time spent in the center versus the periphery, latency to enter

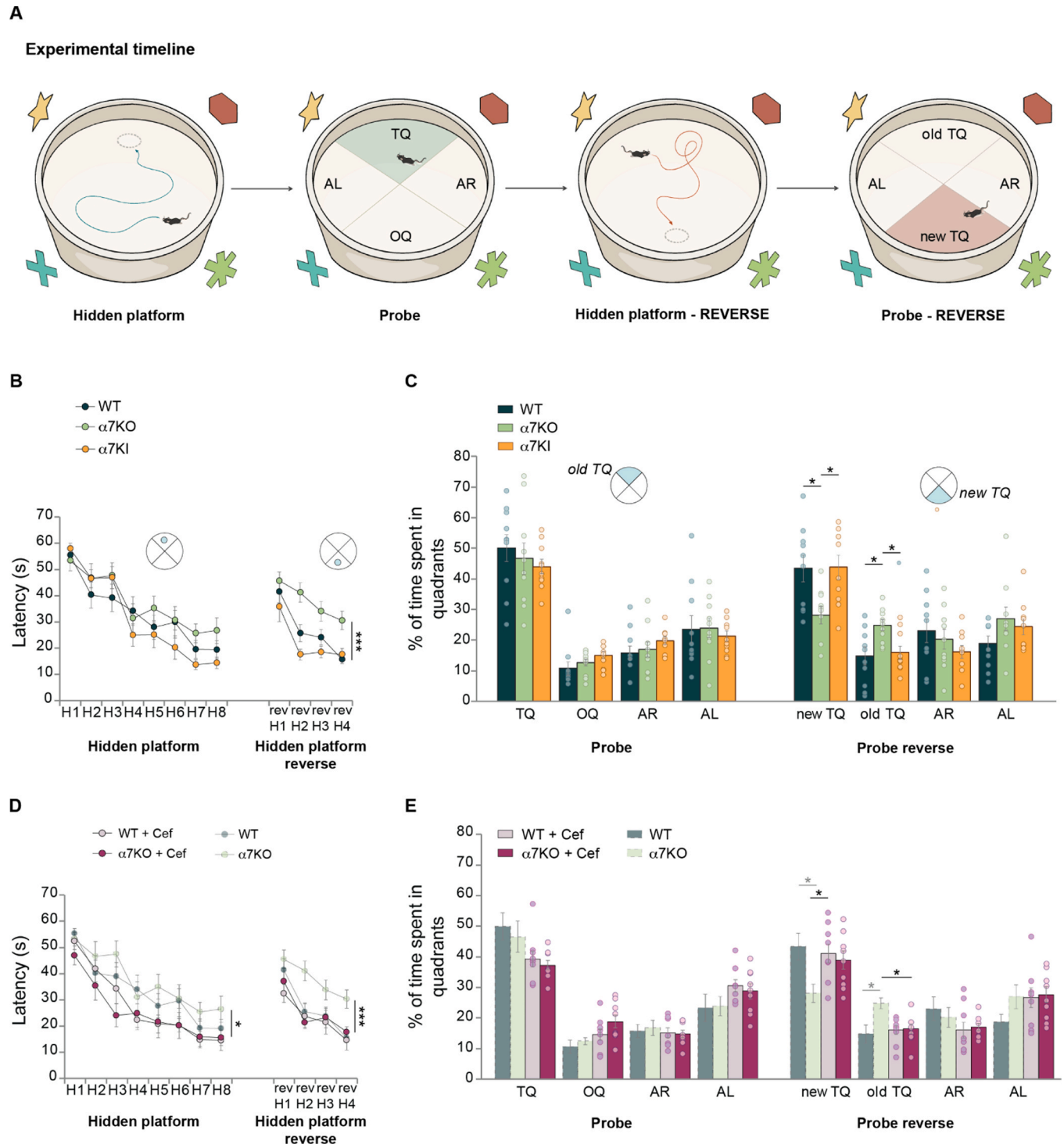

Fig. 6. Alterations of memory flexibility in α7KO mice. A, Schematic representation of the modified Morris Water Maze (MWM) paradigm used to assess memory flexibility. Following acquisition of the initial platform location and a first probe trial, the platform was relocated to a new target quadrant and mice underwent reversal learning training followed by a second probe trial. TQ = target quadrant (old or new), AR = adjacent quadrant right, AL = adjacent quadrant left, OQ = opposite quadrant. **B,** Latency in reaching the submerged platform during the hidden (H1-H8) and the reverse hidden task (rev H1-H4) in WT, α7KO and α7KI-astro mice (n = 10 for each genotype). The circle represents the position of the platform. **C,** Amount of time spent in the four quadrants during the probe (left) and the reverse probe (right) trials. **D,** Effects of the treatment with ceftriaxone in the time spent to reach the submerged platform in the hidden (left) and reverse hidden (right) tests in WT and α7KO mice (n = 9/9). **E,** Effects of the treatment with ceftriaxone in the amount of time spent in the four quadrants during the probe (left) and the reverse probe (right) trials in WT and α7KO mice. *p < 0.05.

the center, and number of entries in the center (Supplementary Fig. 7**B-D**). α7KO mice also showed a normal exploratory behavior, spending a similar amount of time as WT exploring two identical objects (Supplementary Fig. 7**E**). Finally, general locomotor activity, assessed during a 20-min open field session, was comparable between WT and α7KO mice (Supplementary Fig. 7**F**).

Together, these findings indicate that dysfunction of astrocytic α7-nAChRs is associated with deficits in memory flexibility, which are

rescued by astrocytic α7-nAChR re-expression or ceftriaxone treatment.

Thus, dysfunction of astrocytic α7-nAChRs impairs memory flexibility that is rescued by re-expression of α7-nAChRs or a treatment with ceftriaxone.

4. Discussion

In this work, we showed that genetic deletion of α7-nAChRs induces early alterations in glutamate dynamics at hippocampal excitatory synapses due to impaired function and ultrastructural modifications in astrocytes, where the glutamate transporter GLT−1 plays a key role. We also found that α7-nAChR deletion disrupts astrocytic Ca^{2+} signaling, reducing both spontaneous and evoked Ca^{2+} transients that are essential for regulating glutamate handling and synaptic efficacy. Together, these deficits lead to impairments in synaptic transmission, plasticity, and memory flexibility, which are restored through selective re-expression of astrocytic α7-nAChRs, as shown in α7KI-astro models, or by subchronic treatment with ceftriaxone, known to increase GLT−1 levels.

We first confirmed the abundance of α7-nAChRs in the CA1 area, localized in axon terminals, postsynaptic dendrites (Fabian-Fine et al., 2001), and notably in astrocytic processes contacting neuronal synaptic elements. This wide distribution aligns with previous studies showing α7-nAChRs as the predominant subtype in the hippocampus, both in neurons and astrocytes across different models (Graham et al., 2003; Paterson and Nordberg, 2000; Sharma and Vijayaraghavan, 2001; Shen and Yakel, 2012; Yu et al., 2005), and highlights their functional role in modulating neurotransmission, essential for synaptic plasticity and cognitive functions. As expected, α7KO mice, which exhibit a functional alteration of the receptor lacking the binding site for α-BGT (Chen and Patrick, 1997; Orr-Urtreger et al., 1997), presented a significant reduction in α7-nAChR positive synapses and a marked decrease in all synaptic compartments, particularly evident in the astrocytic domain.

Astrocytes play a crucial role in various physiological processes, with their calcium signaling being essential for the release of gliotransmitters, such as glutamate, and finely tuned modulation of synaptic activity (Araque et al., 2014; Bazargani and Attwell, 2016). While much of the previous research has focused on the role of presynaptic neuronal α7-nAChRs that provide the calcium influx needed for glutamate release or inducing depolarization (Koukouli and Maskos, 2015), these receptors also exert a role in glial cells. For example, activation of α7-nAChRs by epibatidine increased glutamate release from mouse gliosomes (Patti et al., 2007), and astrocytic α7-nAChRs modulate glutamate release in response to physiological concentrations of Aβ (Lee et al., 2014). In hippocampal astrocytes, α7-nAChR stimulation evokes rapid intracellular Ca^{2+} elevations, primarily via Ca^{2+}-induced Ca^{2+} release from internal stores (Shen and Yakel, 2012), an effect blocked by α-bungarotoxin (Sharma and Vijayaraghavan, 2001). In vivo, acetylcholine from septo-hippocampal projections activates hippocampal astrocytes trough nAChRs (Pabst et al., 2016), and astrocytic α7-nAChRs drive vesicular D-serine release in the hippocampus (Papouin et al., 2017).

Here, using confocal and 2PLSM for calcium imaging, we observed significant differences in calcium transients between astrocytes in WT and α7KO mice. Spontaneous calcium activity was reduced in both the soma and surrounding territories of α7KO astrocytes, with distinct characteristics possibly related to the spatial localization and function of both the soma and the surrounding territories (Ding et al., 2022). In the soma, a key region for integrating calcium signals, only a few α7KO astrocytes exhibited spontaneous calcium activity, which was reduced in amplitude. In the territories, known to mediate synaptic interactions, initiate signal integration and regulate neurotransmitter uptake and gliotransmitter release (Arizono et al., 2020; Benoit et al., 2025; Lia et al., 2021), a marked reduction in the number of calcium events was observed in α7KO astrocytes compared to controls.

The malfunction of α7-nAChRs also impaired calcium transients typically observed after stimulation with NA or ATP. NA impacts astrocyte calcium activity via α1ARs in several brain regions (Ding et al., 2013; Paukert et al., 2014; Speggiorin et al., 2024), including the hippocampus (Duffy and MacVicar, 1995). ATP, a well-known physiological initiator of calcium waves in astrocytes (Burnstock et al., 2011), primarily acts through P2Y purinergic receptors.

Both ATP and NA activate Gq proteins and inositol 1,4,5-trisphosphate (IP3) signaling, resulting in Ca^{2+} release from intracellular stores. We found that the amplitude of Ca^{2+} events was reduced in both NA-stimulated brain slices and in ATP-stimulated cultured astrocytes. Moreover, α7-nAChR dysfunction prevented the increase in the frequency of Ca^{2+} events in surrounding territories evoked by NA. Although further investigation is needed, we may speculate that α7-nAChRs are critical for replenishing calcium necessary for subsequent release by molecules acting through IP3, such as NA and ATP. The key role of astrocytic α7-nAChRs in these processes was further supported by experiments performed in α7KI-astro models, where selective re-expression of astrocytic α7-nAChRs restored both spontaneous and NA-evoked calcium transients in hippocampal slices.

Glutamate released into the synaptic cleft must be rapidly cleared to prevent spillover and excitotoxicity. This task depends largely on astrocytic excitatory amino acid transporters, particularly GLT−1, the dominant subtype in the hippocampus. Impairment of GLT−1 leads to extracellular glutamate accumulation and neuronal stress, conditions associated with several neurodegenerative disorders, including Alzheimer's disease (AD). In α7KO mice, two-photon glutamate imaging revealed elevated extracellular glutamate peaks after double-pulse stimulation, that was normalized in slices from α7KI-astro mice. We previously reported that paired-pulse facilitation, a measure of neurotransmitter release, was not affected in hippocampal slices from young α7KO mice (Tropea et al., 2021). The slow off kinetics of the glutamate sensor (Marvine et al., 2018) and the fast glutamate uptake suggest that glutamate fluorescence peaks are primarily modulated by rapid binding to glutamate transporters. Therefore, our data indicate a defect in glutamate uptake at the release sites of α7KO mice, as only the fluorescence peak is altered while the decay, which is dependent on glutamate spillover to extrasynaptic sites, remains unaffected. Treatment with the GLT−1 blocker TBOA increased the decay in both WT and α7KO slices, but especially in the latters, while only raised the glutamate peak in α7KO slices. These data indicate that α7KO mice already display altered GLT−1 function, and further inhibition worsens the deficit. In addition, TBOA abolished the different response to double stimuli between α7KO and WT slices, suggesting a functional alteration of GLT−1 in α7KO mice. This was confirmed by increased extracellular glutamate levels in resting α7KO astrocytes in culture, along with reduced Na^+ influx coupled to glutamate uptake in glutamate-stimulated astrocytes.

We also investigated the spatial relationship between α7-nAChRs and GLT−1. Most of the existing work has been conducted in the context of nicotine dependence (Alasmari et al., 2022), showing, for example, that chronic nicotine exposure and nicotine-seeking behavior can alter GLT−1 expression in the brain (Alasmari et al., 2022; Namba et al., 2020). Here, ultrastructural studies revealed that α7-nAChRs and GLT−1 colocalized in astrocytic processes that contact synapses, particularly at the membrane. The absence of functional α7-nAChRs led to a reduction in GLT−1-positive synapses, particularly those involving astrocytic leaflets at asymmetric synapses, and a displacement of astrocytic processes away from synaptic sites. Previous studies showed that defective glutamate clearance due to mislocalized GLT−1 in astrocytes can cause excessive glutamatergic transmission and glutamate accumulation in the extracellular space (Capuani et al., 2016; Parker et al., 2021), which aligns with the increased extracellular glutamate we observed in the medium of α7KO cultured astrocytes. Reduced GLT−1-positive synapses also aligns with increased glutamate peaks, but not decays, that we observed with 2PLSM imaging. Our data also suggest that nAChRs play a role in astrocyte remodeling. Indeed, it has been shown that blocking nAChRs with MLA before nicotine treatment prevented the changes in the length and number of astrocytic processes

(Aryal et al., 2021). Thus, the proper functioning of astrocytic α7-nAChRs is essential not only for the correct expression and localization of GLT−1 but also for maintaining astrocytic leaflets close to synaptic sites, ensuring efficient glutamate uptake by GLT−1 once glutamate is released.

These molecular and structural alterations resulted in clear functional consequences. α7KO mice displayed impaired long-term depression (LTD) consistently with previous studies demonstrating that alterations in GLT−1 distribution and density are involved in the regulation of LTD (Omrani et al., 2009), particularly during periods of intense neuronal activity. In addition, astrocyte–neuron communication has emerged as an important regulator of synaptic plasticity (Durkee et al., 2021), and astrocytic Ca^{2+} signaling is required for CA3–CA1 NMDAR-dependent LTD in the hippocampus (Navarrete et al., 2019). Therefore, the combined alteration of astrocytic Ca^{2+} transients and disruption of GLT−1 organization in α7KO mice likely contribute to the LTD impairment observed.

Consistent with our previous findings (Tropea et al., 2021), we did not detect alterations in hippocampal LTP in young α7KO mice. Indeed, hippocampal LTP deficits emerged only at later ages, together with the development of AD-like pathological features. Notably, the synaptic consequences of α7-nAChR deletion have not been entirely consistent across studies. Previous reports have described heterogeneous alterations in hippocampal plasticity and cognition in α7KO mice, with differences in the onset and nature of the observed phenotypes. For example, age-dependent impairments in hippocampal function have been reported in older α7KO mice (Ma et al., 2014), whereas hippocampal LTP phenotypes have been shown to vary according to genetic background (Freund et al., 2016). Developmental compensation in constitutive KO models may further contribute to this variability.

The impairment of LTD in α7KO slices was accompanied by an increase of synaptic fatigue after intense and repetitive stimulation, linked to the depletion of the RRP and subsequent replenishment of vesicles, suggesting a reduced availability of glutamate during sustained synaptic activity. Such alterations may be linked to disruptions in glutamate dynamics regulated by astrocytes, whose proper functioning is essential for vesicle refilling at neuronal level. These impairments were particularly evident during prolonged stimulation, such as LTD and synaptic fatigue, where the increased demand for glutamate highlights the importance of efficient recycling mechanisms. The specific role of α7-nAChRs in these mechanisms was confirmed as these deficits were fully restored upon re-expression of astrocytic α7-nAChRs in α7KI-astro mice. Interestingly, treatment with ceftriaxone resulted in a slower recovery, likely because ceftriaxone primarily enhances GLT−1 expression which regulates extracellular glutamate levels by increasing buffering activity (Diamond and Jahr, 1997; Herman and Jahr, 2007), rather than facilitating the extracellular-facing conformation required for glutamate/Na^+/H^+ binding and transport cycle (Vandenberg and Ryan, 2013).

At the behavioral level, young α7KO mice showed a reduction of hippocampal memory flexibility. Cognitive flexibility, the ability to adjust thoughts and behavior in response to changing circumstances, relies on memories of past experiences, which contain both unique details and common patterns, to guide decisions even when the situation does not exactly match the original event. This ability enables faster learning and more effective decision-making, and it is essential for adapting to new environments and challenges. Our results indicate that young α7KO mice displayed normal acquisition and retention of the original platform location, suggesting preserved spatial learning and reference memory, consistent with the absence of detectable LTP deficits. In contrast, these mice exhibited a selective impairment in reversal learning and memory flexibility, paralleling the deficit in hippocampal LTD.

Indeed, LTD has emerged as a critical form of synaptic plasticity critical in tasks requiring the modification or elimination of previously learned information. Disruptions in LTD impair reversal learning and behavioral flexibility (Dong et al., 2013; Sangha et al., 2005), suggesting that it is necessary for depotentiation of synapses from previous memory traces, thus allowing the storage of new memories. Our findings suggest that both the loss of LTD and memory flexibility can be attributed to early changes in glutamate dynamics driven by astrocytic dysfunction of α7-nAChRs and GLT−1. In fact, as LTD, memory flexibility deficits were fully rescued by re-expression of α7-nAChRs in astrocytes and ceftriaxone treatment.

It should be noted that cholinergic signaling contributes to a broad range of behavioral functions, including attention, motivation, arousal and exploratory behavior (Hasselmo and Sarter, 2011; Picciotto et al., 2012). Although in our experimental conditions we did not detect alterations in visual performance, exploratory behavior or general locomotion, not all behavioral functions influenced by cholinergic signaling were directly assessed.

Sex-dependent behavioral effects of α7-nAChR deletion have been reported in specific experimental paradigms (Nacer et al., 2021; Otto and Yakel, 2019). Although we did not detect significant sex-dependent effects in the present study, these analyses were limited by the relatively small number of animals per sex and should therefore be interpreted with caution.

Notably, α7KO mice develop an age-dependent AD-like phenotype, with amyloid and tau pathology emerging around 12 months of age (Tropea et al., 2021). This is consistent with evidence from both experimental models and patients showing reduced expression or function of α7-nAChRs in AD (Guan et al., 2000; Marutle et al., 1999). In the present study, the alterations reported occur at 3–6 months of age, well before the onset of overt AD pathology, suggesting that the α7-nAChR/GLT−1 astrocytic dysfunction may represent one of the earliest cellular events predisposing hippocampal circuits to later synaptic failure and consequent cognitive decline. Chronic disruption of α7-nAChR–dependent signaling may progressively weaken glutamate regulation and synaptic adaptability, thereby lowering the threshold for subsequent neurodegenerative processes.

Astrocytic α7-nAChRs therefore emerge as essential regulators of calcium signaling, GLT−1 activity, and astrocyte–synapse organization. Their proper function maintains efficient glutamate clearance and preserves the balance between excitation and depression required for adaptive synaptic plasticity. Disruption of this regulation compromises glutamate dynamics and synaptic flexibility and may create the conditions that, over time, allow for the development of neurodegenerative pathology.

Lead contact

Request for further information and resources should be directed to and will fulfilled by the lead contact Daniela Puzzo (danypuzzo@yahoo.it).

CRediT authorship contribution statement

Maria Rosaria Tropea: Conceptualization, Investigation, Validation, Formal analysis, Visualization, Writing – original draft, Writing – review & editing. **Marcello Melone**: Conceptualization, Investigation, Validation, Formal analysis, Visualization, Funding acquisition, Writing – original draft, Writing – review & editing. **Roberto Piacentini**: Conceptualization, Investigation, Validation, Formal analysis, Visualization, Writing – original draft, Writing – review & editing. **Alessandro Di Spiezio**: Investigation, Validation, Formal analysis, Visualization. **Manuela Tore**: Investigation. **Roberta Carmela Trovato**: Investigation, Formal analysis. **Valeria Vacanti**: Investigation. **Luca Bragina**: Investigation, Formal analysis. **Giulia Puliatti**: Investigation. **Martina Albini**: Investigation. **Beatrice Cannata**: Investigation. **Sara Ben Abid**: Investigation. **Nicole Tonesi**: Investigation. **Angela Chiavegato**: Investigation. **Micaela Zonta**: Investigation, Validation, Formal analysis, Visualization, Writing – original draft, Writing – review & editing.

Cristian Ripoli: Investigation, Methodology, Validation, Formal analysis, Visualization, Writing – original draft, Writing – review & editing. **Gabriele Losi**: Conceptualization, Formal analysis, Writing – original draft, Writing – review & editing, Resources, Supervision, Funding acquisition. **Claudio Grassi**: Conceptualization, Formal analysis, Writing – review & editing, Resources, Supervision, Funding acquisition. **Fiorenzo Conti**: Conceptualization, Formal analysis, Writing – review & editing, Resources, Supervision, Funding acquisition. **Daniela Puzzo**: Conceptualization, Formal analysis, Visualization, Writing – original draft, Writing – review & editing, Resources, Supervision, Funding acquisition, Data curation, Project administration.

Funding

This work was supported by Italian Ministry of University and Research PRIN 2020AMLXHH to M.M., G.L., C.G. and D.P.; Next Generation EU "Age-It—Ageing well in an ageing society" project (PE0000015), NRRP —PE8—Mission 4, C2, Intervention 1.3, F33C2200049006 IRCCS INRCA to F.C. and M.M.; and Italian Ministry of Health "Ricerca Corrente 2025-27" (Oasi Research Institute-IRCCS to D.P.).

Declaration of Competing Interest

The authors declare that they have no known competing financial interests or personal relationships that could have appeared to influence the work reported in this paper.

Acknowledgements

We thank Roberto Colangeli for helpful suggestions on electrophysiological experiments; Paolo Pozzi, Miriam Cavagnini and Irene Incerti for valuable help in setting up 2PLSM glutamate imaging experiments. We thank the Center for Advanced Preclinical in vivo Research (CAPiR) of the University of Catania for behavioral studies.

Appendix A. Supporting information

Supplementary data associated with this article can be found in the online version at doi:10.1016/j.pneurobio.2026.102943.

Data availability

Data will be made available on request.

References

Alasmari, F., Sari, D.B., Alhaddad, H., Al-Rejaie, S.S., Sari, Y., 2022. Interactive role of acid sensing ion channels and glutamatergic system in opioid dependence. Neurosci. Biobehav. Rev. 135, 104581. https://doi.org/10.1016/j.neubiorev.2022.104581.

Amorini, A.M., Lazzarino, G., Di Pietro, V., Signoretti, S., Lazzarino, G., Belli, A., Tavazzi, B., 2017. Severity of experimental traumatic brain injury modulates changes in concentrations of cerebral free amino acids. J. Cell. Mol. Med. 21, 530–542. https://doi.org/10.1111/jcmm.12998.

Araque, A., Carmignoto, G., Haydon, P.G., Oliet, S.H., Robitaille, R., Volterra, A., 2014. Gliotransmitters travel in time and space. Neuron 81, 728–739. https://doi.org/10.1016/j.neuron.2014.02.007.

Arizono, M., Inavalli, V.V.G.K., Panatier, A., Pfeiffer, T., Angibaud, J., Levet, F., Ter Veer, M.J.T., Stobart, J., Bellocchio, L., Mikoshiba, K., Marsicano, G., Weber, B., Oliet, S.H.R., Nägerl, U.V., 2020. Structural basis of astrocytic Ca2+ signals at tripartite synapses. Nat. Commun. 11, 1906. https://doi.org/10.1038/s41467-020-15648-4.

Aryal, S.P., Fu, X., Sandin, J.N., Neupane, K.R., Lakes, J.E., Grady, M.E., Richards, C.I., 2021. Nicotine induces morphological and functional changes in astrocytes via nicotinic receptor activity. Glia 69, 2037–2053. https://doi.org/10.1002/glia.24011.

Babiec, W.E., Guglietta, R., Jami, S.A., Morishita, W., Malenka, R.C., O'Dell, T.J., 2014. Ionotropic NMDA receptor signaling is required for the induction of long-term depression in the mouse hippocampal CA1 region. J. Neurosci. 34, 5285–5290. https://doi.org/10.1523/JNEUROSCI.5419-13.2014.

Bazargani, N., Attwell, D., 2016. Astrocyte calcium signaling: the third wave. Nat. Neurosci. 19, 182–189. https://doi.org/10.1038/nn.4201.

Benoit, L., Hristovska, I., Liaudet, N., Jouneau, P.H., Fertin, A., de Ceglia, R., Litvin, D.G., Di Castro, M.A., Jevtic, M., Zalachoras, I., Kikuchi, T., Telley, L., Bergami, M., Usson, Y., Hisatsune, C., Mikoshiba, K., Pernet-Gallay, K., Volterra, A., 2025. Astrocytes functionally integrate multiple synapses via specialized leaflet domains. Cell 188, 6453–6472. https://doi.org/10.1016/j.cell.2025.08.036.

Bragina, L., Conti, F., 2018. Expression of neurofilament subunits at neocortical glutamatergic and GABAergic synapses. Front. Neuroanat. 12, 74. https://doi.org/10.3389/fnana.2018.00074.

Burnstock, G., Krugel, U., Abbracchio, M.P., Illes, P., 2011. Purinergic signalling: from normal behaviour to pathological brain function. Prog. Neurobiol. 95, 229–274. https://doi.org/10.1016/j.pneurobio.2011.08.006.

Capuani, C., Melone, M., Tottene, A., Bragina, L., Crivellaro, G., Santello, M., Casari, G., Conti, F., Pietrobon, D., 2016. Defective glutamate and K+ clearance by cortical astrocytes in familial hemiplegic migraine type 2. EMBO Mol. Med. 8, 967–986. https://doi.org/10.15252/emmm.201505944.

Chen, W., Mahadomrongkul, V., Berger, U.V., Bassan, M., DeSilva, T., Tanaka, K., Irwin, N., Aoki, C., Rosenberg, P.A., 2004. The glutamate transporter GLT1a is expressed in excitatory axon terminals of mature hippocampal neurons. J. Neurosci. 24, 1136–1148. https://doi.org/10.1523/JNEUROSCI.1586-03.2004.

Chen, D., Patrick, J.W., 1997. The alpha-bungarotoxin-binding nicotinic acetylcholine receptor from rat brain contains only the alpha7 subunit. J. Biol. Chem. 272, 24024–24029. https://doi.org/10.1074/jbc.272.38.24024.

Chen, N., Sugihara, H., Sharma, J., Perea, G., Petravicz, J., Le, C., Sur, M., 2012. Nucleus basalis-enabled stimulus-specific plasticity in the visual cortex is mediated by astrocytes. Proc. Natl. Acad. Sci. USA 109, E2832–E2841. https://doi.org/10.1073/pnas.1206557109.

Danbolt, N.C., 2001. Glutamate uptake. Prog. Neurobiol. 65, 1–105. https://doi.org/10.1016/s0301-0082(00)00067-8.

Dani, J.A., Bertrand, D., 2007. Nicotinic acetylcholine receptors and nicotinic cholinergic mechanisms of the central nervous system. Annu. Rev. Pharmacol. Toxicol. 163, 699–729. https://doi.org/10.1146/annurev.pharmtox.47.120505.105214.

DeFelipe, J., Marco, P., Busturia, I., Merchán-Pérez, A., 1999. Estimation of the number of synapses in the cerebral cortex: methodological considerations. Cereb. Cortex 9, 722–773. https://doi.org/10.1093/cercor/9.7.722.

Diamond, J.S., Jahr, C.E., 1997. Transporters buffer synaptically released glutamate on a submillisecond time scale. J. Neurosci. 17, 4672–4687. https://doi.org/10.1523/JNEUROSCI.17-12-04672.1997.

Ding, F., Liang, S., Li, R., Yang, Z., He, Y., Yang, S., Duan, Q., Zhang, J., Lyu, J., Zhou, Z., Huang, M., Wang, H., Li, J., Yang, C., Wang, Y., Gong, M., Chen, S., Jia, H., Chen, X., Liao, X., Fu, L., Zhang, K., 2022. Astrocytes exhibit diverse Ca2+ changes at subcellular domains during brain aging. Front. Aging Neurosci. 14, 1029533. https://doi.org/10.3389/fnagi.2022.1029533.

Ding, F., O'Donnell, J., Thrane, A.S., Zeppenfeld, D., Kang, H., Xie, L., Wang, F., Nedergaard, M., 2013. α1-Adrenergic receptors mediate coordinated Ca2+ signaling of cortical astrocytes in awake, behaving mice. Cell. Calcium 54, 387–394. https://doi.org/10.1016/j.ceca.2013.09.001.

Dong, Z., Bai, Y., Wu, X., Li, H., Gong, B., Howland, J.G., Huang, Y., He, W., Li, T., Wang, Y.T., 2013. Hippocampal long-term depression mediates spatial reversal learning in the Morris water maze. Neuropharmacology 64, 65–73. https://doi.org/10.1016/j.neuropharm.2012.06.027.

Duffy, S., MacVicar, B.A., 1995. Adrenergic calcium signaling in astrocyte networks within the hippocampal slice. J. Neurosci. 15, 5535–5550. https://doi.org/10.1523/JNEUROSCI.15-08-05535.1995.

Durkee, C., Kofuji, P., Navarrete, M., Araque, A., 2021. Astrocyte and neuron cooperation in long-term depression. Trends Neurosci. 44, 837–848. https://doi.org/10.1016/j.tins.2021.07.004.

Fabian-Fine, R., Skehel, P., Errington, M.L., Davies, H.A., Sher, E., Stewart, M.G., Fine, A., 2001. Ultrastructural distribution of the alpha7 nicotinic acetylcholine receptor subunit in rat hippocampus. J. Neurosci. 21, 7993–8003. https://doi.org/10.1523/JNEUROSCI.21-20-07993.2001.

Freund, R.K., Graw, S., Choo, K.S., Stevens, K.E., Leonard, S., Dell'Acqua, M.L., 2016. Genetic knockout of the α7 nicotinic acetylcholine receptor gene alters hippocampal long-term potentiation in a background strain-dependent manner. Neurosci. Lett. 627, 1–6. https://doi.org/10.1016/j.neulet.2016.05.043.

Graham, A.J., Ray, M.A., Perry, E.K., Jaros, E., Perry, R.H., Volsen, S.G., Bose, S., Evans, N., Lindstrom, J., Court, J.A., 2003. Differential nicotinic acetylcholine receptor subunit expression in the human hippocampus. J. Chem. Neuroanat. 25, 97–113. https://doi.org/10.1016/s0891-0618(02)00100-x.

Guan, Z.Z., Zhang, X., Ravid, R., Nordberg, A., 2000. Decreased protein levels of nicotinic receptor subunits in the hippocampus and temporal cortex of patients with Alzheimer's disease. J. Neurochem. 74, 237–243. https://doi.org/10.1046/j.1471-4159.2000.0740237.x.

Gulisano, W., Melone, M., Ripoli, C., Tropea, M.R., Li Puma, D.D., Giunta, S., Cocco, S., Marcotulli, D., Origlia, N., Palmeri, A., Arancio, O., Conti, F., Grassi, C., Puzzo, D., 2019. Neuromodulatory action of picomolar extracellular Aβ42 oligomers on presynaptic and postsynaptic mechanisms underlying synaptic function and memory. J. Neurosci. 39, 5986–6000. https://doi.org/10.1523/JNEUROSCI.0163-19.2019.

Hasselmo, M.E., Sarter, M., 2011. Modes and models of forebrain cholinergic neuromodulation of cognition. Neuropsychopharmacology 36, 52–73. https://doi.org/10.1038/npp.2010.104.

Herde, M.K., Bohmbach, K., Domingos, C., Vana, N., Komorowska-Müller, J.A., Passlick, S., Schwarz, I., Jackson, C.J., Dietrich, D., Schwarz, M.K., Henneberger, C., 2020. Local efficacy of glutamate uptake decreases with synapse size. Cell. Rep. 32, 108182. https://doi.org/10.1016/j.celrep.2020.108182.

Herman, M.A., Jahr, C.E., 2007. Extracellular glutamate concentration in hippocampal slice. J. Neurosci. 27, 9736–9741. https://doi.org/10.1523/JNEUROSCI.3009-07.2007.

Kim, J.I., Lee, H.R., Sim, S.E., Baek, J., Yu, N.K., Choi, J.H., Ko, H.G., Lee, Y.S., Park, S. W., Kwak, C., Ahn, S.J., Choi, S.Y., Kim, H., Kim, K.H., Backx, P.H., Bradley, C.A., Kim, E., Jang, D.J., Lee, K., Kim, S.J., Zhuo, M., Collingridge, G.L., Kaang, B.K., 2011. PI3Kγ is required for NMDA receptor-dependent long-term depression and behavioral flexibility. Nat. Neurosci. 14, 1447–1454. https://doi.org/10.1038/nn.2937.

Koukouli, F., Maskos, U., 2015. The multiple roles of the α7 nicotinic acetylcholine receptor in modulating glutamatergic systems in the normal and diseased nervous system. Biochem. Pharmacol. 97, 378–387. https://doi.org/10.1016/j.bcp.2015.07.018.

Lawal, O., Ulloa Severino, F.P., Eroglu, C., 2022. The role of astrocyte structural plasticity in regulating neural circuit function and behavior. Glia 70, 1467–1483. https://doi.org/10.1002/glia.24191.

Lee, L., Kosuri, P., Arancio, O., 2014. Picomolar amyloid-β peptides enhance spontaneous astrocyte calcium transients. J. Alzheimers Dis. 38, 49–62. https://doi.org/10.3233/JAD-130740.

Li Puma, D.D., Ripoli, C., Puliatti, G., Pastore, F., Lazzarino, G., Tavazzi, B., Arancio, O., Piacentini, R., Grassi, C., 2022. Extracellular tau oligomers affect extracellular glutamate handling by astrocytes through downregulation of GLT-1 expression and impairment of NKA1A2 function. Neuropathol. Appl. Neurobiol. 48, e12811. https://doi.org/10.1111/nan.12811.

Lia, A., Di Spiezio, A., Vitalini, L., Tore, M., Puja, G., Losi, G., 2023. Ion channels and ionotropic receptors in astrocytes: physiological functions and alterations in Alzheimer's disease and glioblastoma. Life 13, 2038. https://doi.org/10.3390/life13102038.

Lia, A., Henriques, V.J., Zonta, M., Chiavegato, A., Carmignoto, G., Gómez-Gonzalo, M., Losi, G., 2021. Calcium signals in astrocyte microdomains, a decade of great advances. Front. Cell. Neurosci. 15, 673433. https://doi.org/10.3389/fncel.2021.673433.

Lin, H., Vicini, S., Hsu, F.C., Doshi, S., Takano, H., Coulter, D.A., Lynch, D.R., 2010. Axonal α7 nicotinic ACh receptors modulate presynaptic NMDA receptor expression and structural plasticity of glutamatergic presynaptic boutons. Proc. Natl. Acad. Sci. USA 107, 16661–16666. https://doi.org/10.1073/pnas.1007397107.

Ma, L., Turner, D., Zhang, J., Wang, Q., Wang, M., Shen, J., Zhang, S., Wu, J., 2014. Deficits of synaptic functions in hippocampal slices prepared from aged mice null α7 nicotinic acetylcholine receptors. Neurosci. Lett. 570, 97–101. https://doi.org/10.1016/j.neulet.2014.04.018.

Marutle, A., Warpman, U., Bogdanovic, N., Lannfelt, L., Nordberg, A., 1999. Neuronal nicotinic receptor deficits in Alzheimer patients with the Swedish amyloid precursor protein 670/671 mutation. J. Neurochem. 72, 1161–1169. https://doi.org/10.1046/j.1471-4159.2000.0721161.x.

Marvin, J.S., Scholl, B., Wilson, D.E., Podgorski, K., Kazemipour, A., Müller, J.A., Schoch, S., Quiroz, F.J.U., Rebola, N., Bao, H., Little, J.P., Tkachuk, A.N., Cai, E., Hantman, A.W., Wang, S.S., DePiero, V.J., Borghuis, B.G., Chapman, E.R., Dietrich, D., DiGregorio, D.A., Fitzpatrick, D., Looger, L.L., 2018. Stability, affinity, and chromatic variants of the glutamate sensor iGluSnFR. Nat. Methods 15, 936–939. https://doi.org/10.1038/s41592-018-0300-z.

Melone, M., Bellesi, M., Conti, F., 2009. Synaptic localization of GLT-1a in the rat somatic sensory cortex. Glia 57, 108–117. https://doi.org/10.1002/glia.20744.

Melone, M., Ciriachi, C., Pietrobon, D., Conti, F., 2019. Heterogeneity of astrocytic and neuronal GLT-1 at cortical excitatory synapses, as revealed by its colocalization with Na+/K+-ATPase α isoforms. Cereb. Cortex 29, 3331–3350. https://doi.org/10.1093/cercor/bhy203.

Nacer, S.A., Letsinger, A.C., Otto, S.L., et al., 2021. Loss of α7 nicotinic acetylcholine receptors in GABAergic neurons causes sex-dependent decreases in radial glia-like cell quantity and impairments in cognitive and social behavior. Brain Struct. Funct. 226, 365–379. https://doi.org/10.1007/s00429-020-02179-3.

Namba, M.D., Kupchik, Y.M., Spencer, S.M., Garcia-Keller, C., Goenaga, J.G., Powell, G. L., Vicino, I.A., Hogue, I.B., Gipson, C.D., 2020. Accumbens neuroimmune signaling and dysregulation of astrocytic glutamate transport underlie conditioned nicotine-seeking behavior. Addict. Biol. 25, e12797. https://doi.org/10.1111/adb.12797.

Navarrete, M., Cuartero, M.I., Palenzuela, R., Draffin, J.E., Konomi, A., Serra, I., Colié, S., Castaño-Castaño, S., Hasan, M.T., Nebreda, Á.R., Esteban, J.A., 2019. Astrocytic p38α MAPK drives NMDA receptor-dependent long-term depression and modulates long-term memory. Nat. Commun. 10, 2968. https://doi.org/10.1038/s41467-019-10830-9.

Omrani, A., Melone, M., Bellesi, M., Safiulina, V., Aida, T., Tanaka, K., Cherubini, E., Conti, F., 2009. Up-regulation of GLT-1 severely impairs LTD at mossy fibre–CA3 synapses. J. Physiol. 587, 4575–4588. https://doi.org/10.1113/jphysiol.2009.177881.

Orr-Urtreger, A., Göldner, F.M., Saeki, M., Lorenzo, I., Goldberg, L., De Biasi, M., Dani, J. A., Patrick, J.W., Beaudet, A.L., 1997. Mice deficient in the alpha7 neuronal nicotinic acetylcholine receptor lack alpha-bungarotoxin binding sites and hippocampal fast nicotinic currents. J. Neurosci. 17, 9165–9171. https://doi.org/10.1523/JNEUROSCI.17-23-09165.1997.

Otto, S.L., Yakel, J.L., 2019. The α7 nicotinic acetylcholine receptors regulate hippocampal adult neurogenesis in a sexually dimorphic fashion. Brain Struct. Funct. 224, 829–846. https://doi.org/10.1007/s00429-018-1799-6.

Pabst, M., Braganza, O., Dannenberg, H., Hu, W., Pothmann, L., Rosen, J., Mody, I., van Loo, K., Deisseroth, K., Becker, A.J., Schoch, S., Beck, H., 2016. Astrocyte intermediaries of septal cholinergic modulation in the hippocampus. Neuron 90, 853–865. https://doi.org/10.1016/j.neuron.2016.04.003.

Palmeri, A., Mammana, L., Tropea, M.R., Gulisano, W., Puzzo, D., 2016. Salidroside, a bioactive compound of Rhodiola rosea, ameliorates memory and emotional behavior in adult mice. J. Alzheimers Dis. 52, 65–75. https://doi.org/10.3233/JAD-151159.

Papouin, T., Dunphy, J.M., Tolman, M., Dineley, K.T., Haydon, P.G., 2017. Septal cholinergic neuromodulation tunes the astrocyte-dependent gating of hippocampal NMDA receptors to wakefulness. Neuron 94, 840–854. https://doi.org/10.1016/j.neuron.2017.04.021.

Parker, P.D., Suryavanshi, P., Melone, M., Sawant-Pokam, P.A., Reinhart, K.M., Kaufmann, D., Theriot, J.J., Pugliese, A., Conti, F., Shuttleworth, C.W., Pietrobon, D., Brennan, K.C., 2021. Non-canonical glutamate signaling in a genetic model of migraine with aura. Neuron 109, 611–628.e8. https://doi.org/10.1016/j.neuron.2020.11.018.

Paterson, D., Nordberg, A., 2000. Neuronal nicotinic receptors in the human brain. Prog. Neurobiol. 61, 75–111. https://doi.org/10.1016/s0301-0082(99)00045-3.

Patti, L., Raiteri, L., Grilli, M., Zappettini, S., Bonanno, G., Marchi, M., 2007. Evidence that alpha7 nicotinic receptor modulates glutamate release from mouse neocortical gliosomes. Neurochem. Int. 51, 1–7. https://doi.org/10.1016/j.neuint.2007.03.003.

Paukert, M., Agarwal, A., Cha, J., Doze, V.A., Kang, J.U., Bergles, D.E., 2014. Norepinephrine controls astroglial responsiveness to local circuit activity. Neuron 82, 1263–1270. https://doi.org/10.1016/j.neuron.2014.04.038.

Peters, A., Palay, S.L., Webster, H.F., 1991. The Fine Structure of the Nervous System: Neurons and Their Supporting Cells. Oxford University Press.

Piacentini, R., Li Puma, D.D., Mainardi, M., Lazzarino, G., Tavazzi, B., Arancio, O., Grassi, C., 2017. Reduced gliotransmitter release from astrocytes mediates tau-induced synaptic dysfunction in cultured hippocampal neurons. Glia 65, 1302–1316. https://doi.org/10.1002/glia.23163.

Picciotto, M.R., Higley, M.J., Mineur, Y.S., 2012. Acetylcholine as a neuromodulator: cholinergic signaling shapes nervous system function and behavior. Neuron 76, 116–129. https://doi.org/10.1016/j.neuron.2012.08.036.

Pirttimaki, T.M., Codadu, N.K., Awni, A., Pratik, P., Nagel, D.A., Hill, E.J., Dineley, K.T., Parri, H.R., 2013. α7 nicotinic receptor-mediated astrocytic gliotransmitter release: Aβ effects in a preclinical Alzheimer's mouse model. PLoS One 8, e81828. https://doi.org/10.1371/journal.pone.0081828.

Puliatti, G., Renna, P., Battistoni, M., Piacentini, R., Ripoli, C., Grassi, C., 2026. AAV. PHP.eB-based strategies for precise modulation of α7 nicotinic acetylcholine receptor in neurons and astrocytes in the adult mouse brain. Sci. Rep. 16, 15439. https://doi.org/10.1038/s41598-026-46279-2.

Rao, P., Yallapu, M.M., Sari, Y., Fisher, P.B., Kumar, S., 2015. Designing novel nanoformulations targeting glutamate transporter excitatory amino acid transporter 2: implications in treating drug addiction. J. Pers. Nanomed. 1, 3–9.

Ripoli, C., Dagliyan, O., Renna, P., Pastore, F., Paciello, F., Sollazzo, R., Rinaudo, M., Battistoni, M., Martini, S., Tramutola, A., Sattin, A., Barone, E., Saneyoshi, T., Fellin, T., Hayashi, Y., Grassi, C., 2023. Engineering memory with an extrinsically disordered kinase. Sci. Adv. 9, eadh1110. https://doi.org/10.1126/sciadv.adh1110.

Rothstein, J.D., Martin, L., Levey, A.I., Dykes-Hoberg, M., Jin, L., Wu, D., Nash, N., Kuncl, R.W., 1994. Localization of neuronal and glial glutamate transporters. Neuron 13, 713–725. https://doi.org/10.1016/0896-6273(94)90038-8.

Rothstein, J.D., Patel, S., Regan, M.R., Haenggeli, C., Huang, Y.H., Bergles, D.E., Jin, L., Dykes Hoberg, M., Vidensky, S., Chung, D.S., Toan, S.V., Bruijn, L.I., Su, Z.Z., Gupta, P., Fisher, P.B., 2005. Beta-lactam antibiotics offer neuroprotection by increasing glutamate transporter expression. Nature 433, 73–77. https://doi.org/10.1038/nature03180.

Sangha, S., Narayanan, R.T., Bergado, J.A., Huston, J.P., 2005. Impairing forgetting by preventing new learning and memory. Behav. Neurosci. 119, 787–796. https://doi.org/10.1037/0735-7044.119.3.787.

Sharma, G., Vijayaraghavan, S., 2001. Nicotinic cholinergic signaling in hippocampal astrocytes involves calcium-induced calcium release from intracellular stores. Proc. Natl. Acad. Sci. U. S. A. 98, 4148–4153. https://doi.org/10.1073/pnas.071540198.

Shen, J.X., Yakel, J.L., 2012. Functional α7 nicotinic ACh receptors on astrocytes in rat hippocampal CA1 slices. J. Mol. Neurosci. 48, 14–21. https://doi.org/10.1007/s12031-012-9719-3.

Smaga, I., Fierro, D., Mesa, J., Filip, M., Knackstedt, L.A., 2020. Molecular changes evoked by the beta-lactam antibiotic ceftriaxone across rodent models of substance use disorder and neurological disease. Neurosci. Biobehav. Rev. 115, 116–130. https://doi.org/10.1016/j.neubiorev.2020.05.016.

Speggiorin, M., Chiavegato, A., Zonta, M., Gómez-Gonzalo, M., 2024. Characterization of the astrocyte calcium response to norepinephrine in the ventral tegmental area. Cells 14, 24. https://doi.org/10.3390/cells14010024.

Takahashi, K., Foster, J.B., Lin, C.L., 2015. Glutamate transporter EAAT2: regulation, function, and potential as a therapeutic target for neurological and psychiatric disease. Cell. Mol. Life Sci. 72, 3489–3506. https://doi.org/10.1007/s00018-015-1937-8.

Takata, N., Mishima, T., Hisatsune, C., Nagai, T., Ebisui, E., Mikoshiba, K., Hirase, H., 2011. Astrocyte calcium signaling transforms cholinergic modulation to cortical plasticity in vivo. J. Neurosci. 31, 18155–18165. https://doi.org/10.1523/JNEUROSCI.5289-11.2011.

Tropea, M.R., Li Puma, D.D., Melone, M., Gulisano, W., Arancio, O., Grassi, C., Conti, F., Puzzo, D., 2021. Genetic deletion of α7 nicotinic acetylcholine receptors induces an age-dependent Alzheimer's disease-like pathology. Prog. Neurobiol. 206, 102154. https://doi.org/10.1016/j.pneurobio.2021.102154.

Tropea, M.R., Melone, M., Li Puma, D.D., Vacanti, V., Aceto, G., Bandiera, B., Trovato, R. C., Torrisi, S.A., Leggio, G.M., Palmeri, A., D'Ascenzo, M., Conti, F., Grassi, C., Puzzo, D., 2024. Blockade of dopamine D3 receptors improves hippocampal synaptic function and rescues age-related cognitive phenotype. Aging Cell. 23, e14291. https://doi.org/10.1111/acel.14291.

Tropea, M.R., Sanfilippo, G., Giannino, F., Davì, V., Gulisano, W., Puzzo, D., 2022. Innate preferences affect results of object recognition task in wild type and Alzheimer's disease mouse models. J. Alzheimers Dis. 85, 1343–1356. https://doi.org/10.3233/JAD-215209.

Vandenberg, R.J., Ryan, R.M., 2013. Mechanisms of glutamate transport. Physiol. Rev. 93, 1621–1657. https://doi.org/10.1152/physrev.00007.2013.

Wang, Y., DelRosso, N.V., Vaidyanathan, T.V., Cahill, M.K., Reitman, M.E., Pittolo, S., Mi, X., Yu, G., Poskanzer, K.E., 2019. Accurate quantification of astrocyte and neurotransmitter fluorescence dynamics for single-cell and population-level physiology. Nat. Neurosci. 22, 1936–1944. https://doi.org/10.1038/s41593-019-0492-2.

Yu, W.F., Guan, Z.Z., Bogdanovic, N., Nordberg, A., 2005. High selective expression of alpha7 nicotinic receptors on astrocytes in the brains of patients with sporadic Alzheimer's disease and patients carrying Swedish APP 670/671 mutation: a possible association with neuritic plaques. Exp. Neurol. 192, 215–225. https://doi.org/10.1016/j.expneurol.2004.12.015.

Zhang, H., Gong, B., Liu, S., Fa', M., Ninan, I., Staniszewski, A., Arancio, O., 2005. Synaptic fatigue is more pronounced in the APP/PS1 transgenic mouse model of Alzheimer's disease. Curr. Alzheimer Res. 2, 137–140. https://doi.org/10.2174/1567205053585936.